Time and length scales of polymer melts studied by coarse-grained molecular dynamics simulations

ARTICLE *in* THE JOURNAL OF CHEMICAL PHYSICS · JULY 2002

Impact Factor: 2.95 · DOI: 10.1063/1.1481859

2 AUTHORS:

Johan T Padding
Technische Universiteit Eindhoven
85 PUBLICATIONS **1,441** CITATIONS
SEE PROFILE

Wim J Briels
University of Twente
178 PUBLICATIONS **4,336** CITATIONS
SEE PROFILE

Time and length scales of polymer melts studied by coarse-grained molecular dynamics simulations

J. T. Padding[a] and W. J. Briels[b]
Computational Dispersion Rheology, Department of Applied Physics, University of Twente, P.O. Box 217, 7500 AE Enschede, The Netherlands

(Received 20 February 2002; accepted 8 April 2002)

We present coarse-grained molecular dynamics simulations of linear polyethylene (PE) melts, ranging in chain length from C_{80} to C_{1000}. The employed effective potentials, frictions, and random forces are all derived from detailed molecular dynamics simulations, leaving no adjustable parameters. Uncrossability constraints are introduced in the coarse-grained model to prevent unphysical bond crossings. The dynamic and zero-shear rate rheological properties are investigated and compared with experiment and other simulation work. In the analysis of the internal relaxations we identify a new length scale, called the slowing down length N_s, which is smaller than the entanglement length N_e. The effective segmental friction rapidly increases around N_s leading, at constant density, to a transition in the scaling of the diffusion coefficient from $D \sim N^{-1}$ to $D \sim N^{-2}$, a transition in the scaling of the viscosity from $\eta \sim N$ to $\eta \sim N^{1.8}$, and conspicuous nonexponential relaxation behavior. These effects are attributed to strong local kinetic constraints caused by both chain stiffness and interchain interactions. The onset of nonlocal (entanglement) effects occurs at a chain length of C_{120}. Full entanglement effects are observed only above C_{400}, where the shear relaxation modulus displays a plateau and the single chain coherent dynamic structure factor agrees with the reptation model. In this region the viscosity scales as $\eta \sim N^{3.6}$, the tube diameter is $d \approx 5.4$ nm, the entanglement molecular weight is $M_e \approx 1700$ g/mol, and the plateau modulus is $G_N^0 \approx 2.4$ MPa, all in good agreement with experimental data. © *2002 American Institute of Physics.* [DOI: 10.1063/1.1481859]

I. INTRODUCTION

Long-chain polymer liquids are well-known for their peculiar viscoelastic behavior. The relaxation of stress after a step shear strain at first occurs in a liquidlike fashion, but soon, at least if the molecular weight is sufficiently large, a plateau is reached very similar to what is found in solids and rubbers. In the long run, the remaining stress of course relaxes, as it must in a liquid. The range of time scales associated with these relaxations can be enormous. On the shortest time scales, processes such as atomic bond vibrations and torsional jumps are important, whereas the longest time scales are associated with the escape of chains from entanglements with other, surrounding chains. This escaping time depends strongly on molecular weight and scales approximately with the molecular weight to the power of 3.4, irrespective of the chemical details of the polymer.

Because of the enormously large relaxation times, conventional atomistic molecular dynamics simulations of long-chain polymer melts are practically impossible. Such simulations have been performed only for medium long chains up to about 150 monomers.[1–5] At first glance these simulations seem to indicate that the dynamics and rheology of medium long chains may well be described by the Rouse model.[6] Yet the applicability of this inherently single chain model has been questioned in literature, especially as far as the rheology is concerned, because an important part of the shear stress is observed to arise from the intermolecular interactions.[7–9] Recently, we have shown that interchain interactions are important in the shear relaxation of $C_{120}H_{242}$.[10]

In order to simulate dynamical and rheological behavior of long chains one has to resort to coarse-grained models.[10–16] Usually, the interactions between two coarse objects, called blobs from now on, are chosen such that bond crossings will be energetically unfavorable. The range of the repulsive forces is then necessarily of the order of the maximum separation of two bonded blobs. If one wants to avoid using physically unrealistic models, this sets a severe limit to the number of monomers which may be represented by one blob. Moreover, no systematic method exists to calculate model parameters on the coarse level from atomistic, i.e., chemically realistic simulations. Of course one may fix time and length scales by mapping/adjusting simulation to experimental results, but usually it is doubtful with these models whether one and the same set of mapping parameters is able to describe all experimental data. Recently we proposed a model whose parameters were calculated from a short molecular dynamics simulation.[10,17] A friction ''frequency'' ξ, though, had to be obtained by trial and error while adjusting the results of a mesoscopic simulation with those of an atomistic simulation in the time regime where both are applicable. In the Appendix of the present paper we present a direct way to calculate ξ from microscopic simulations,

[a]Electronic mail: j.t.padding@ct.utwente.nl
[b]Electronic mail: w.j.briels@tn.utwente.nl

thereby turning the whole procedure into an "*ab initio*" calculation. Obviously *ab initio* is not meant in a quantum-chemical sense, but in the sense that we start at the lowest relevant scale for statistical simulations. In statistical physics the interactions between the constituent particles are considered to be a prescribed basic ingredient. (There are two reasons to do *ab initio* quantum-chemical simulations like, e.g., Car and Parrinello simulations: First, if one is interested in restructuring of electronic densities, and second, in cases when no simple interaction model can be formulated and one is obliged to calculate forces on the fly.)

In this paper we present the results of various dynamic properties of polyethylene, obtained by simulations on 7 processors of an SGI Origin 2000 system (UNITE) for more than 1 year. We will focus on the determination of characteristic length scales, particularly the entanglement length, and try to gain insight in the origin of these length scales.

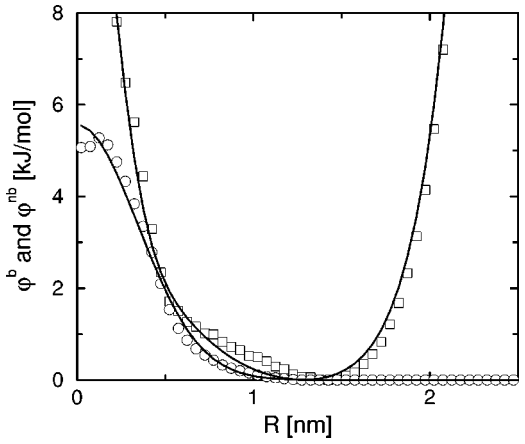

FIG. 1. The potential of mean force between nonbonded (circles) and bonded (squares) blobs. These potentials were obtained from the distribution functions measured in atomistically detailed molecular dynamics simulations of $C_{120}H_{242}$ at the same temperature and density as the current simulations. The solid lines are fits with simple analytical functions, as described in Ref. 10.

II. METHOD

A. Coarse-grained interactions and uncrossability of chains

In the simulation a blob represents the center of mass of λ consecutive monomers. The fundamental difference with some other polymer simulation models, such as the FENE model of Kremer *et al.*,[11] is that λ may be chosen arbitrarily and is not determined afterwards by a mapping procedure to relate the simulation results to experimental values. This is possible because the interaction model is not fixed *a priori*, but derived without any adjustable parameters from short microscopic simulations of the material under consideration. The number of monomers per blob is however not completely arbitrary. If spherical interactions are assumed, λ should not be so large that the size of the blob exceeds the typical diameter of the tube in the reptation picture. In that case, it would be impossible for the model to display a tube of realistic proportions. For practical purposes, λ must not be too small either. In the first place, much is gained if λ is as large as possible to allow for a large integration time step. Secondly, λ must be large enough to be able to treat the complementary $3(\lambda-1)$ coordinates per blob of the microscopic constituents as bath variables, i.e., to take their effects into account through random forces which perturb the time evolution of the blob positions. If the random forces decorrelate much faster than the blob momenta, the random force correlations may be represented by delta functions (Markov approximation) and the equations of motion are of the simplest Langevin-type;

$$M\frac{d^2\mathbf{R}_i}{dt^2}=-\nabla_i\chi-M\xi\frac{d\mathbf{R}_i}{dt}+\mathbf{F}_i^R, \tag{1}$$

where $\mathbf{R}_i$ is the position of blob i, M is its mass, and ξ is the blob friction frequency, related to the random force $\mathbf{F}^R$ through the fluctuation dissipation theorem. In Eq. (1) we have implicitly assumed that the friction on each blob is isotropic and independent of the positions of the other blobs, in which case the friction is a scalar quantity. In the Appendix we describe how this quantity can be calculated from short atomistic simulations. The free energy χ, which is the potential of mean force, can be calculated from

$$\chi(\mathbf{R}^n)=-kT\ln P_n(\mathbf{R}^n). \tag{2}$$

Here P_n is the n-blob distribution function which is determined from the microscopic system by averaging over the bath variables. It is assumed that this distribution can be factorized into independent pairwise and angular parts. At first sight this assumption may seem rather crude, and better methods to estimate the effective interactions are available, such as the method described by McCoy and Curro,[18] who mapped explicit atom onto united atom potentials. However, this method may run into problems if applied to polymers, because two nonbonded blobs which are nevertheless part of the same chain are not independent entities; the interactions between two such blobs are not determined by interactions between the atoms of these blobs alone.[19] Fortunately, the long time dynamics and rheology of polymer chains is dominated not so much by the details of the interactions, but by the fact that chains can not cross each other.

Now, in this work we will investigate polyethylene melts at a temperature of 450 K and a constant density of 0.761 g/cm^3. In a previous paper[10] we argued that a suitable level of coarse-graining for this material is $\lambda=20$, which is well below any reported entanglement length. In atomistic molecular dynamics simulations of a melt of $C_{120}H_{242}$ chains the blob distibution functions were measured. From these we calculated the interaction potentials. The interactions between pairs of bonded and pairs of nonbonded blobs are shown in Fig. 1. Because the degree of coarse-graining is so high, the blobs are rather "empty" and the interactions between blobs are very soft. Consequently, in the mesoscopic simulations based on the above Langevin equation, without additional measures unphysical bond crossings will be probable. To prevent this from happening, a new uncrossability constraint is applied. The idea behind this constraint is to consider the bonds between consecutive blobs to be elastic bands. As soon as two of these elastic bands make contact,

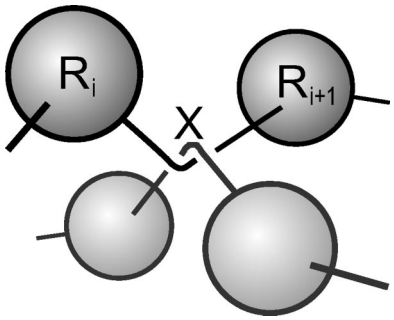

FIG. 2. Sketch of two ''entangled'' parts of chains. At an earlier time, the bonds between the two depicted pairs of blobs tried to cross each other. This caused the uncrossability constraint to insert an ''entanglement'' at the crossing point. Since then the attractive part of the potential between bonded blobs is a function of the path length from blob i, via the entanglement at $\mathbf{X}$, to blob $i+1$.

an ''entanglement'' is created at the crossing position $\mathbf{X}$ which prevents the elastic bands from crossing. This is accomplished by defining the attractive part of the potential between bonded blobs i and $i+1$ to be a function of the path length $L_{i,i+1}$ of the bond, going from one blob (i) to the next $(i+1)$ via the intermediate entanglement,

$$L_{i,i+1}=|\mathbf{R}_i-\mathbf{X}|+|\mathbf{X}-\mathbf{R}_{i+1}|. \tag{3}$$

See Fig. 2 for a sketch of this situation. The position of the entanglement is determined by the requirement that there is always an equilibrium of forces at the entanglement. Of course more than one entanglement per bond is allowed. Details about this and more about the uncrossability constraint can be found in Ref. 10.

We stress that the entanglements are created and annihilated according to the dynamics of the system itself and no network structure is imposed *a priori*. The uncrossability constraints are called ''entanglements'' for simplicity, but they are not the classic entanglements which form a network of effective tubes and attribute to the long time stress. This work is therefore conceptually very different from work of, e.g., Masubuchi *et al.*[20] who coarsegrained at the level of segments between consecutive entanglements, therefore imposing a network of primitive chains. In Sec. III A we will focus on the characteristics of the uncrossability constraints.

B. Equilibration and characterization of the systems under study

In this paper we investigate melts of seven different chain lengths, ranging from $C_{80}H_{162}$ to $C_{1000}H_{2002}$, hereafter referred to as B_4 to B_{50}, after the number of blobs representing one chain. An overview of the systems is given in Table I. In order to avoid significant interactions of a chain with its periodic images, the number of chains in each system was chosen such that the length of the periodic simulation box was at least the root mean squared end-to-end distance of a polymer chain. A similar criterion was adopted by Kremer and Grest.[11] To check finite size effects, they analyzed a melt of FENE chains of length 200 (comparable to our B_{30}) for two system sizes, one with 20 and one with 100 chains. Although the static dimensions of the chains depended slightly on the system size, all dynamic results for both system sizes were found to be the same within the statistical errors. We are therefore confident that the sizes of the systems studied in this work are sufficiently large.

TABLE I. Polymer species, number of blobs N per chain, number of chains n_{chain}, length L of the simulation box, the mean square radius of gyration $\langle R_g^2\rangle$, and mean square end-to-end distance $\langle R_e^2\rangle$ of the systems studied.

Species	N	n_{chain}	L (nm)	$\langle R_g^2\rangle$ (nm^2)	$\langle R_e^2\rangle$ (nm^2)
C_{80}/B_4	4	180	7.61	1.51	10.2
C_{120}/B_6	6	120	7.61	2.51	16.3
C_{200}/B_{10}	10	100	8.49	4.05	25.3
C_{400}/B_{20}	20	80	9.93	9.05	54.9
C_{600}/B_{30}	30	80	11.37	14.9	91.8
C_{800}/B_{40}	40	80	12.51	21.6	132.2
C_{1000}/B_{50}	50	80	13.48	27.2	167.3

Unlike microscopic chains, well-equilibrated initial configurations of mesoscopic chains can be realized with comparative ease due to the softness of the interactions and the possibility to relax the configurations *before* imposing the uncrossability constraint. Initial configurations of the chains were generated according to the distribution functions obtained from microscopic simulations and were placed and oriented randomly in the simulation box. The repulsive force between nonbonded blobs was initially set to 1/10th of its final value in order to gently push blobs with large overlap apart, while allowing all bonds to cross each other. After this initial homogenization, the nonbonded force was gradually increased to reach its final value. The melts were then equilibrated for at least one rotational relaxation time. This was possible because the longest relaxation times of crossing chains are much shorter than those of noncrossing chains.[10] Finally, the uncrossability constraint was switched on. The number of entanglements was monitored and observed to reach an equilibrium value (in an average sense) within a few nanoseconds for *all* systems. Nondiagonal components of the stress tensor were also monitored and found to be zero on average.

To check whether the equilibration of the chain structure was successful at all relevant length scales, the Rouse modes of the chains were studied. For a finite chain of length N these are given by[21]

$$\mathbf{X}_k=\frac{1}{N}\sum_{j=1}^{N} A_{kj}\mathbf{R}_j \quad (k=0,\ldots,N-1), \tag{4}$$

where A_{kj} is defined as

$$A_{kj}=\cos\left[\frac{k\pi}{N}\left(j-\frac{1}{2}\right)\right]. \tag{5}$$

The zeroth Rouse mode is the position of the center-of-mass of the chain. All other modes describe the internal configuration of the chain, mode number k describing a wavelength corresponding to a subchain of N/k blobs. According to Rouse theory, the amplitudes should obey the scaling relation

$$\langle \mathbf{X}_k^2\rangle=\frac{b^2}{8N\sin^2\left(\frac{k\pi}{2N}\right)}. \tag{6}$$

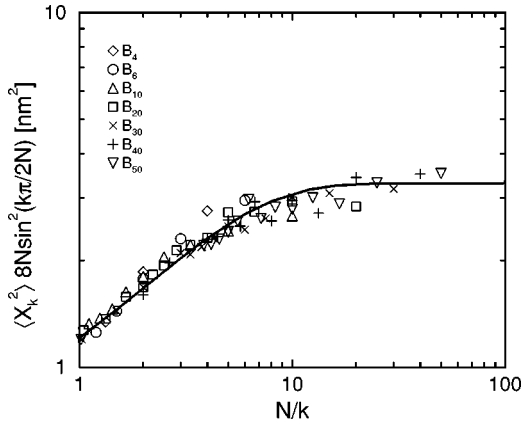

FIG. 3. Rouse amplitudes vs N/k for several values of k and N. The results are scaled such that the data would fall on a horizontal line for ideal chains. The line is a guide to the eye.

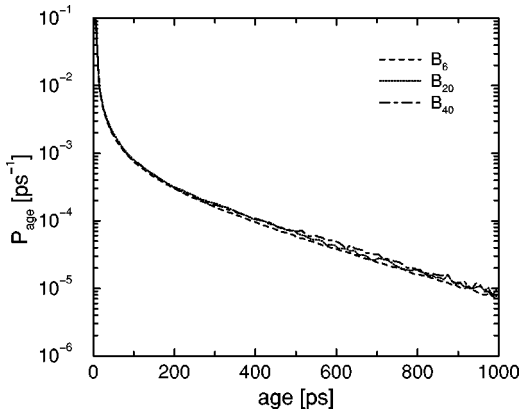

FIG. 4. Probability that an ''entanglement'' (uncrossability constraint) dies at a given age. Effective entanglements, which contribute to the long time stress, are rare but more common than one would estimate from this plot (see text).

We calculated $\langle \mathbf{X}_k^2 \rangle \cdot 8N \sin^2(k\pi/2N)$ for each chain length and mode number. According to Eq. (6), for an ideal chain this should be constant and equal to the square of the statistical segment length b. Our chains however are not ideal, mainly because of the angular potential which gives them some stiffness. The stiffness will have the strongest effect on the smallest length scales, but no effect on the very large length scales where ideal random walk statistics should be obeyed. More importantly, if the systems are well-equilibrated, we expect that the data of all the chains collapse onto one single curve if it is plotted against the natural scale N/k. As can be seen in Fig. 3, this is indeed the case. From the limiting value we can estimate the statistical segment length to be $b^2 \approx 3.3$ nm^2. As can be seen in Table I, the mean square end-to-end distance and mean square radius of gyration of the longest chains obey random walk statistics, i.e., $\langle R_e^2 \rangle = Nb^2$ and $\langle R_g^2 \rangle = \frac{1}{6} Nb^2$. In view of the above, we are confident that all starting configurations have relaxed sufficiently.

III. RESULTS

A. Entanglement characteristics

During the simulations the chains try to cross each other in which case the uncrossability constraint creates entanglements. Entanglements are also annihilated because chains slip off the ends of other chains, they unknot, or simply because chains move apart again.[10] Obviously, the number of entanglements is not constant but fluctuating in time. The long-time average number of entanglements however was found to be constant and equal to 2.5 entanglements per bond in all systems. Many of these entanglements were short-lived. Accordingly, only a few contributed significantly to long time interactions between different chains and therefore to the long time stress. To quantify this, we present in Fig. 4 the probability P_{age} of an entanglement to reach a certain ''age.'' Age is defined here as the time interval between the creation and annihilation of a certain entanglement. There are two prominent features in the plot of P_{age}: (i) After a sharp initial drop the probability decreases exponentially with age. From the slope in the semilogarithmic plot we derive a characteristic decay time of 230 ps. (ii) Somewhat surprisingly, also at the long life times, all curves coincide. This proves that even B_6 behaves as a chain, not as a small molecule. Apparently the influence of the chain ends on the life time of uncrossability constraints is very small.

We expect a larger influence of the chain ends on the *effective* number of entanglements which do get old and contribute significantly to the long time stress. The calculation of the number of such effective entanglements is however complicated by the fact that in determining the age we have disregarded the possibility that two entangled chains, due to some fluctuation, move apart for a very short time after which they entangle again at approximately the same location. Although this would be the same entanglement effectively, it is treated as a new entanglement in the calculation of P_{age}. In this work we will not try to correct for this, for instance by allowing two parts of chains to be separated for a specified maximum time interval and maximum relative displacement, because new and nontrivial variables would need to be introduced. Instead, we will calculate the effective number of entanglements from the influence they have on the dynamic and rheological properties. In the following subsections we will focus on these properties and find that only one in every 15 entanglements will be effective in creating a ''tube,'' i.e., we will find that the classic entanglement length of our model polyethylene is $N_e \approx 6$ blobs.

B. Slowing down of Rouse mode relaxations

In Sec. II we checked the equilibration of the chain structure by analyzing the Rouse mode amplitudes, Eqs. (4)–(6). We will now focus on the time dependence of these Rouse modes because they reveal the relaxation dynamics at different length scales. Within the Rouse model, for ideal chains, each of the modes relaxes independently and exponentially with a relaxation time τ_k,

$$C_k(t) \equiv \langle \mathbf{X}_k(t) \cdot \mathbf{X}_k(0) \rangle / \langle \mathbf{X}_k^2 \rangle = \exp(-t/\tau_k), \tag{7}$$

$$\tau_k^{-1} = 4W \sin^2\left(\frac{k\pi}{2N}\right), \tag{8}$$

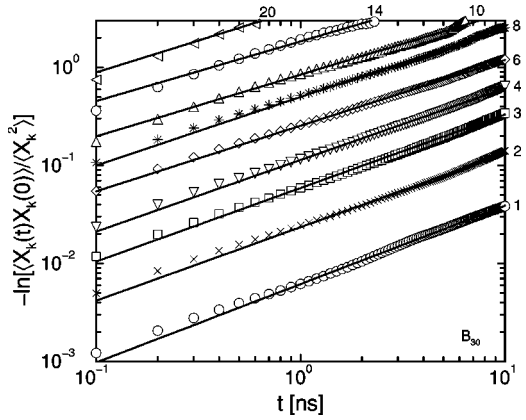

FIG. 5. Rouse mode relaxations in the B_{30} system, scaled as $-\ln[C_k(t)]$ on a double logarithmic scale to extract the stretching parameters β_k. Solid lines are the fits. Mode numbers are given along the top and right-hand side of the plot.

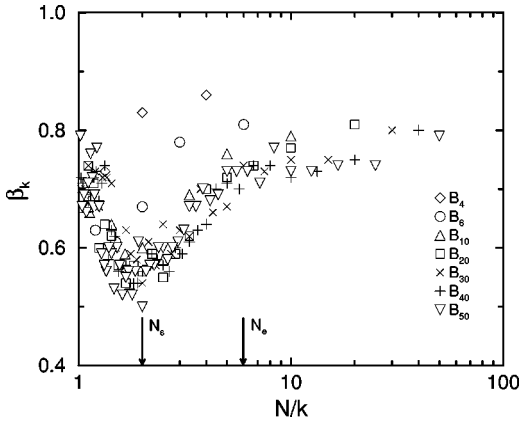

FIG. 7. Stretching parameters β_k vs N/k for several values of k and N. A distinct minimum is observed at $N/k=N_s\approx 2$.

where the relaxation rate W is a characteristic frequency of the Rouse model and is given by

$$W=\frac{3kT}{M\xi b^2}. \tag{9}$$

For realistic polymer chains, however, it is not expected that the Rouse modes are the normal modes (in a dynamic sense; the static cross-correlations *are* zero), because the nonbonded interactions and uncrossability constraints modify the equations of motion and make them highly nonlinear.[22,23] As a consequence, the Rouse modes may no longer relax exponentially. As was already observed in other simulation work,[1,23,24] we find that the Rouse mode autocorrelations of polymer chains can better be described by a stretched exponential form,

$$C_k(t)=\exp[-(t/\tau_k^*)^{\beta_k}], \tag{10}$$

where the relaxation times τ_k^* and stretching parameters β_k depend on mode number k and on the chain length. The Rouse modes were measured and fitted to Eq. (10) by calculating minus the natural logarithm of the normalized autocorrelations and plotting them on a double-logarithmic scale. A typical example is given in Fig. 5, where this procedure has been applied to several Rouse modes of the B_{30} system. Consistent with Eq. (10) straight lines result, with a slope equal to β_k and an intercept (at some time $t>0$) proportional to $1/\tau_k^*$. In Fig. 6 we show the original data, together with the fits from Fig. 5, on a semilogarithmic scale. Notice that the fits do well in describing the data and that the nonexponentiality of the data is strongest around $k=14$. In Fig. 7 we have plotted β_k for all chain lengths and all mode numbers against the mode wavelength N/k. The data more or less collapse on to the same curve, at least for $N>6$ and N/k smaller than about 6. At the smallest length scales β_k is approximately 0.7. Then a minimum of approximately 0.5 occurs around $N/k\approx 2$, after which β_k increases again to a value of approximately 0.8 at the largest scale of each chain.

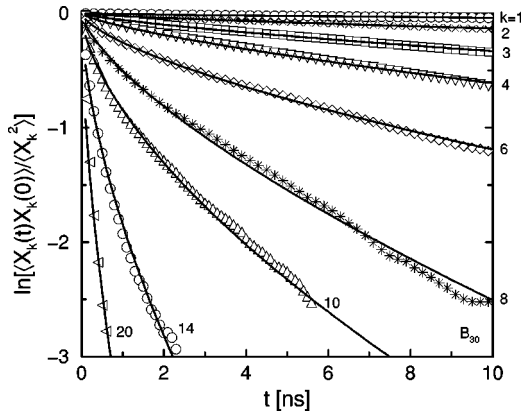

FIG. 6. Rouse mode relaxations in the B_{30} system, scaled as $\ln[C_k(t)]$ on a linear scale, showing the nonexponentiality of the simulation data. Solid lines are the fits. The fit quality for $k=1$ is better appreciated in Fig. 5.

The nonexponential relaxation of the Rouse modes is not specific to our model. Shaffer placed polymers on a lattice and applied uncrossability constraints.[23] He also found deviations from exponential behavior, very similar to what we find. Shaffer interpreted the devation of β_k from unity to reflect the severity of kinetic constraints. He suggested that the results may also be interpreted in the framework of the coupling model of Ngai and co-workers, in which the degree of nonexponentiality is associated with the cooperativity that is required for configurational relaxation in the presence of entanglement constraints.[25] With these interpretations in mind, Fig. 7 suggests that the effect of kinetic constraints and/or the required cooperativity is most severe around $N/k\approx 2$. We will introduce a separate symbol for this length scale: N_s, where the *s* stands for ''slowing down,'' because the dynamics of the chain is strongly slowing down at this length scale. Notice that we do not interpret this length scale as the entanglement length N_e from classic reptation theory.

The slowdown of dynamics at various length scales becomes clearly perceptible if we analyze the Rouse mode relaxation times. Note that the parameter τ_k^* is not very useful in itself because the instant relaxation rate at any time t depends on all three t, τ_k^*, and β_k. In analogy with Shaffer's work, we calculate the effective relaxation times as time integrals over the normalized relaxation functions. From Eq. (10) we find

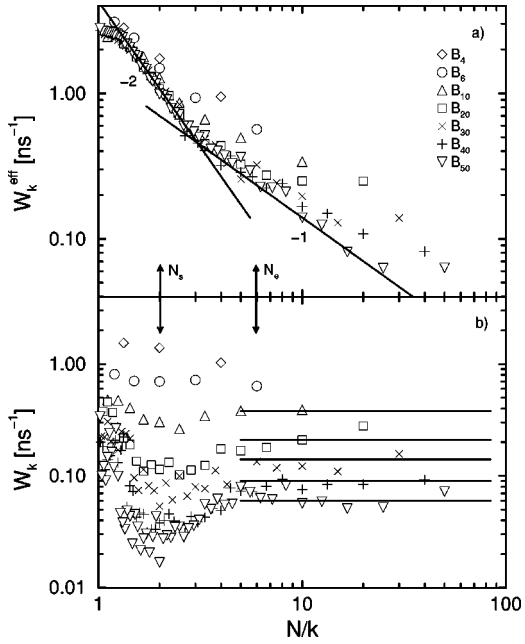

FIG. 8. Effective Rouse relaxation rates (a) and terminal Rouse relaxation rates (b) vs N/k for several values of k and N. The lines in (a) show the scaling regimes $\tau_k^{\mathrm{eff}} \sim N^4/k^4$ and $\tau_k^{\mathrm{eff}} \sim N^3/k^3$. The lines in (b) show the $\tau_k^l \sim N^{3.5}/k^2$ scaling for scales larger than N_e, in agreement with reptation theory.

$$\tau_k^{\mathrm{eff}} = \int_0^\infty C_k(t)dt = \int_0^\infty \exp[-(t/\tau_k^*)^{\beta_k}]dt = \frac{\tau_k^*}{\beta_k}\Gamma(1/\beta_k), \tag{11}$$

where $\Gamma(x)$ is the gamma function. The corresponding effective Rouse rate is defined as

$$W_k^{\mathrm{eff}} = \left[4\tau_k^{\mathrm{eff}} \sin^2\left(\frac{k\pi}{2N}\right)\right]^{-1}, \tag{12}$$

which, in the case of Rouse chains, is a constant and equal for all chain lengths. In Fig. 8(a) we have plotted the effective Rouse rates for all chain lengths and all mode numbers against the mode wavelength N/k. It is interesting to see that the data of each chain length follow the same ''universal'' curve until they depart to reach a plateau at a value which differs for each chain length. The universal curve has the following characteristics:

(1) Initially the effective Rouse rate is constant, which means that the effective relaxation times scale like predicted in Eq. (8). This regime is very small, only up to about 1.5 blobs. In this respect we can say that only the very small length scales behave Rouse-type.
(2) Then there is a sharp drop in the effective Rouse rate. The curve has an apparent minimal slope of -2 in the neighborhood of N_s. This means that the effective relaxation times scale like $\tau_k^{\mathrm{eff}} \sim (N/k)^4$ in this regime.
(3) A regime with slope -1 starts at about $1.5N_s$ and ends when a plateau is reached. The effective relaxation times in this regime scale like $\tau_k^{\mathrm{eff}} \sim (N/k)^3$.

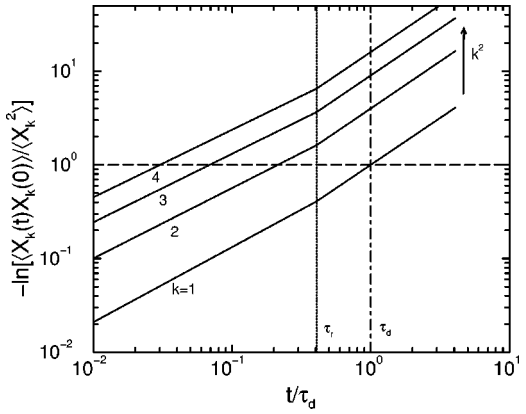

FIG. 9. Relaxation of the Rouse modes (schematically) for different mode numbers. The chain has relaxed along the primitive path at τ_r, after which all modes relax exponentially. At the disentanglement time τ_d the relaxation of the first mode is by definition $1/e$ (dashed line). The long time relaxation times scale as $1/k^2$ with mode number.

Both the second and third regimes are quite distinct from the predictions of both Rouse ($\sim N^2/k^2$) and reptation ($\sim N^3/k^2$) models. We will return to this in the discussion. The occurrence of a plateau in the W_k^{eff} data is in agreement with the reptation model although other models which also predict a plateau cannot be ruled out, such as the generalized Rouse approach by Hess.[26] The original reptation theory predicts that the relaxation time of a Rouse mode k with $N/k > N_e$ is enhanced by a factor $3N/N_e$ compared to the Rouse model,[27] i.e., the plateau of W_k should decrease proportional to N^{-1}. The plateau values in Fig. 8(a) decrease somewhat faster, approximately with $N^{-1.5}$. This can be explained by including contour length fluctuations in the reptation theory.[27] The chain ends have a large effect on the relaxation times in chains which are not far above the entanglement length, such as our chains.

C. Disentanglement times

Contrary to what we would expect, the plateau in Fig. 8(a) is restricted to the first few modes, even for the longer chains. The same observation was made by Shaffer.[23] We should keep in mind, however, that we have calculated effective relaxation times, Eq. (11), which are largely dominated by the relaxations at short times, where the correlations still differ appreciably from zero. If we want to obtain information about their long time behavior, we are forced to investigate the correlation functions themselves. According to reptation theory, the Rouse mode correlation functions decay exponentially, with characteristic times $\tau_k \sim N^3/k^2$, at times larger than the time τ_r it takes for the chain to relax along its own primitive path, and for values of k such that $N/k > N_e$. In the original application of the reptation model τ_r was assumed to be the Rouse time τ_R of a hypothetical chain which does not feel the tube constraints. We shall refrain from this interpretation and continue to use τ_r for the time when reptation sets in. Since at times larger than the disentanglement time τ_d each chain will have found a completely new environment, the Rouse mode correlation functions will

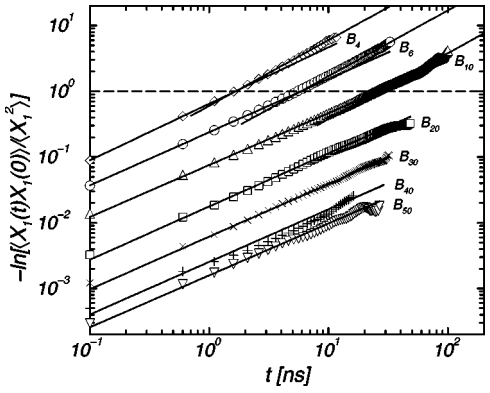

FIG. 10. Relaxation of the first Rouse mode for different values of N (symbols). The data are scaled in the same way as in Fig. 5. Solid lines are fits to the relaxation regime $t<\tau_r$, with slope $\beta_1=0.8$ (except for the B_4 system), and the regime $t>\tau_r$, with slope 1, respectively. The horizontal dashed line indicates where $C_1(t)=1/e$.

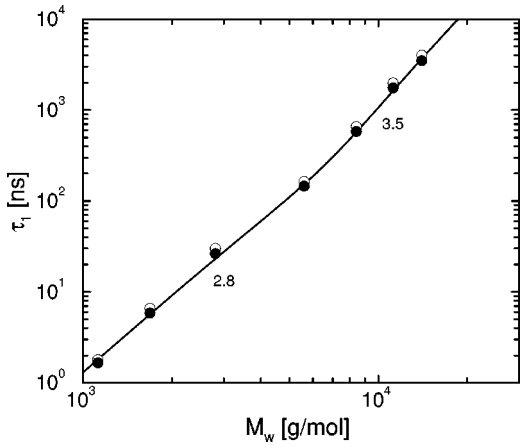

FIG. 11. Estimated disentanglement times τ_d (filled circles) and effective relaxation times (open circles) as estimated by Eq. (11) vs molecular weight M_w. The solid line is a guide to the eye.

decay exponentially at these times, and consequently $\tau_r \leqslant \tau_d$. The Rouse mode correlation functions then behave according to

$$C_k(t)=\begin{cases}\exp[-(t/\tau_k^*)^{\beta_k}] & \text{for } t<\tau_r,\\ \exp[-(t/\tau_k^l)] & \text{for } t>\tau_r,\end{cases} \tag{13}$$

where τ_k^l is the terminal (long time) relaxation time. The exponential decay time of the first mode is the above mentioned disentanglement time, i.e., $\tau_1^l=\tau_d$. $C_k(t)$ then decays as schematically depicted in Fig. 9. Notice that at time $t=\tau_d$, $C_1(t)$ has decayed to $1/e$ of its original value at $t=0$. $C_k(t)$ with mode numbers k larger than 1 decay faster.

We expect that for the shorter chains, although already strongly influenced by entanglements, the primitive paths are still too short for reptation to be applicable, and that *consequently* "$\tau_r\approx\tau_d$." Only for very long chains will τ_r substantially differ from τ_d. In Fig. 10 we investigate the relaxation of the first Rouse mode of each chain length. The data for $N<20$ clearly display a crossover from a short time relaxation with $\beta_1\approx 0.8$ to a long time exponential relaxation. For each of these chain lengths, the two asymptotes intersect at $-\ln C_1(t)=1$ (dashed line in Fig. 10), i.e., when the normalized autocorrelation has decayed to $1/e$. So indeed we find that for these chain lengths we have $\tau_r=\tau_d$, i.e., the chain has never completely relaxed along its primitive path until a new environment is found. For $N\geqslant 6$ times τ_r are certainly larger than the Rouse times τ_R of unentangled chains. Values of τ_R can be estimated from our previous work where we investigated chains which were able to cross each other.[10] The effective Rouse rate of large scale modes was found to be $W\approx 1.2\ \text{ns}^{-1}$. This yields estimates of τ_R listed in the second column of Table II. Only for $N=4$ there is agreement between τ_r and τ_R. For both $N=6$ and $N=10$ the nonexponential decay persists much longer than τ_R. We assume that the same will hold for $20\leqslant N\leqslant 50$, although no rigorous proof can be given, because the exponential time regime could not be reached. Still, all these chain lengths show the same stretching parameter, $\beta_1=0.8$ (solid lines in Fig. 10). A deviation is visible in the data of the B_{40} system. Because this deviation is not visible when $N=30$ nor when $N=50$, we expect that it is incidental and will disappear after longer averaging. An upper limit of τ_d can be estimated by extrapolating $-\ln C_1(t)$ up to the time where it is equal to 1 (see Fig. 9). Since our longest chain length is only about 8 times the entanglement length τ_r will not be very different from τ_d and consequently the real disentanglement time will by very close to this estimate. The scaling of the estimated τ_d with molecular weight is investigated in Fig. 11 (filled circles). Two regimes can be distinguished, with scaling exponents 2.8 and 3.5, respectively. The latter value is markedly larger than the pure reptation prediction of 3, but in agreement with the theory if contour length fluctuations are taken into account.

Next we investigate the long time relaxation of intermediate modes. A typical plot is given in Fig. 12, where $k=1$, 2, 3, and 4 results of the B_{10} system are shown. Although statistical uncertainties arise in the data when $C_k(t)\approx 0$, we clearly find that for each mode $k>1$ the nonexponential be-

TABLE II. Calculated Rouse times τ_R (ns) of crossing chains and effective relaxation times τ_k^{eff} (ns) of noncrossing chains for various mode numbers k.

N	τ_R	$k=1$	2	3	4	5	6	7	8	9	10	15	19	29	39	49
4	1.42	1.62	0.29	0.10												
6	3.10	5.67	1.05	0.34	0.14	0.09										
10	8.5	25.3	4.99	1.83	0.84	0.39	0.21	0.15	0.11	0.10						
20	34	140	38	16.6	8.0	3.9	2.7	1.68	1.02	0.61	0.47	0.13	0.09			
30	76	559	162	52	24.0	11.6	10.2	5.9	3.4	2.5	1.86	0.49	0.21	0.10		
40	135	1687	359	121	61	27.3	20.5	12.7	9.1	5.6	5.3	1.59	0.57	0.14	0.09	
50	211	3367	925	346	128	73	34	23.4	17.8	10.9	7.2	2.37	1.33	0.27	0.11	0.09

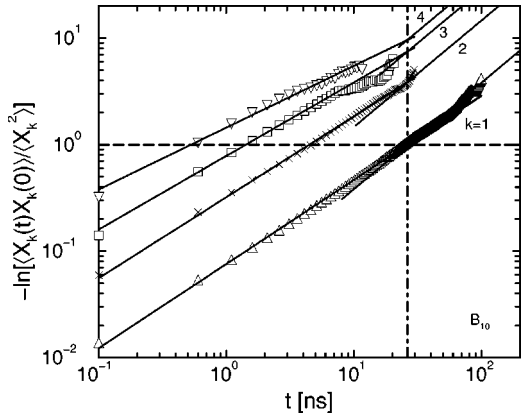

FIG. 12. Relaxation of modes $k=1$, 2, 3, and 4 for $N=10$ (symbols). The data are scaled in the same way as in Fig. 5. Solid lines are fits and extrapolations to the relaxation regimes $t<\tau_r$ and $t>\tau_r$, respectively. The horizontal line indicates where $C_k(t)=1/e$, the vertical dotted–dashed line is at $t=\tau_r$.

havior persists far beyond the time when $C_k(t)=1/e$. We are unable to follow the relaxation into the exponential regime, but we assume that the nonexponential behavior persists up to τ_r, as was stated in Eq. (13). The terminal relaxation time τ_k^l of Rouse mode k can be derived from known τ_k^* and β_k data by equating the two regimes in Eq. (13) at $t=\tau_r$, resulting in

$$\tau_k^l=\tau_r\left(\frac{\tau_k^*}{\tau_r}\right)^{\beta_k}. \tag{14}$$

The reptation scaling $\tau_k\sim N^3/k^2$ must be valid in the regime $t>\tau_r$. This is checked in Fig. 8(b), where we plot the Rouse mode relaxation rates based upon the terminal relaxation times. Indeed, a broad reptation-like plateau is observed for each chain length if $N/k>N_e\approx 6$. A small dip occurs at scales below the entanglement length N_e, with a minimum around $N_s\approx 2$, consistent with the observations made before on the stretching parameter β_k. Contrary to Fig. 8(a), the Rouse rates do not converge to some universal curve at the smallest scales. This indicates that Eq. (13) does not hold for scales far below N_e. This will have no practical consequences in future applications of Eq. (13), however, because the correlation functions of these smallest scale modes are completely negligible in the time regime $t>\tau_r$.

Effective relaxation times can be calculated again as integrals over $C_k(t)$, but now in two parts, one before τ_r and one after. These effective relaxation times are given in Table II and were actually used to calculate the effective Rouse rates in Fig. 8(a). It should be noted, that these relaxation rates are essentially equal to those calculated with Eq. (11) for mode numbers two and higher, because the contribution to the integral for times $t>\tau_r$ is negligibly small. Only the effective relaxation time of the first mode is somewhat overestimated by Eq. (11), as can be seen in Fig. 11.

D. Slowing down of diffusion

In the previous subsections we have analyzed the internal relaxations of the polymer chains. Now we will investigate the mobility of blobs and centers of mass. Before we do this, we will summarize the reptation model predictions. In the reptation model the effects of the surrounding chains on the dynamics of a polymer chain are incorporated effectively by forcing a Rouse chain to move inside a tube formed by entanglements with other chains. A constant friction with the background and no other constraints besides the tube are assumed. At short times, a blob does not know about any tube constraints. The mean square displacement of a blob, defined as

$$g(t)=\frac{1}{N}\sum_{i=1}^{N}\langle[\mathbf{R}_i(t)-\mathbf{R}_i(0)]^2\rangle, \tag{15}$$

will therefore behave Rouse-type and scale like $t^{1/2}$. [We note that for even shorter times, shorter than the fastest relaxation time of the chain τ_0, $g(t)$ is proportional to t.] When the blob has moved a distance comparable to the tube diameter, the only way for the chain to relax further is along the primitive path. This is supposed to happen at the entanglement time τ_e. The chain next moves, still in a Rouse-type fashion, but now along a quasi-one-dimensional path, leading to the famous $t^{1/4}$ power law for the mean square displacement of the blobs. After a certain time τ_r the chain has relaxed along its tube. In the reptation model this time is the Rouse time τ_R. Next, assuming that the tube does not change appreciably, an overal diffusion along the tube is predicted, leading to a second $t^{1/2}$ regime. Finally, after the disentanglement time τ_d, the chain has managed to escape its old tube and create a new one, and the blobs start to diffuse.

It is generally believed now that the reptation model, in its essentials, correctly picks up the physical behavior of polymer melts. This will be confirmed in the following subsections where we will show that ''coarse'' quantities, such as the shear relaxation modulus, can well be described by the reptation model. The constant friction approximation, however, is too strict. In reality, as we have seen in the previous subsections, an increasing effective friction is associated with increasing length scales. The increase is strongest around N_s. Because $N_s<N_e$ we expect that the blobs effectively slow down even *before* they have moved a tube diameter distance. The typical time scale τ_s at which this may happen can be estimated from Fig. 8(a) and Eq. (12) by assuming it to be the effective relaxation time of a subchain of length N_s. This yields a ''slowing down time'' $\tau_s\approx 0.47$ ns. In Fig. 13, the blob mean square displacement of several chain lengths is plotted against time. Although for $N\geqslant 20$ we did not reach the diffusion limit, it is clear that longer chains are increasingly slowed down. For B_{50} an effective minimal slope of about 0.4 is measured. Perhaps less clear is the onset of this regime, which agrees with the predicted slowing down time τ_s. The preceding regime, where normal Rouse behavior $[g(t)\sim t^{1/2}]$ is observed, turns out to be quite narrow, however. This is a consequence of the fact that we have coarse-grained relatively far, making the fastest relaxation time of the chain come close to the slowing down time τ_s. If we had coarse-grained even further, combining 40 instead of 20 monomers into one blob, this $t^{1/2}$ regime would not have been observed at all. The fastest relaxation time, according to Eq. (12), is given by

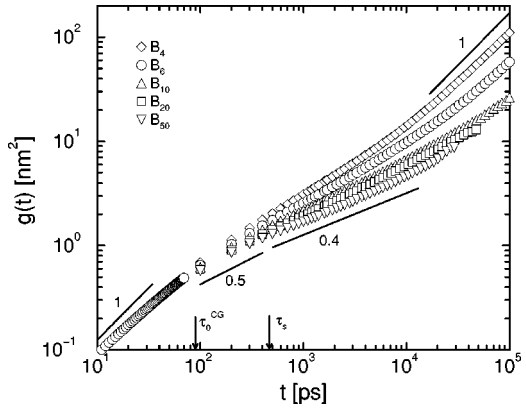

FIG. 13. Blob mean square displacement $g(t)$ vs t averaged over all blobs for five different values of N. The fastest possible relaxation time in the coarse-grained system, Eq. (16), is indicated by the arrow labeled with τ_0^{CG}. The slowing down time is indicated by the arrow labeled with τ_s.

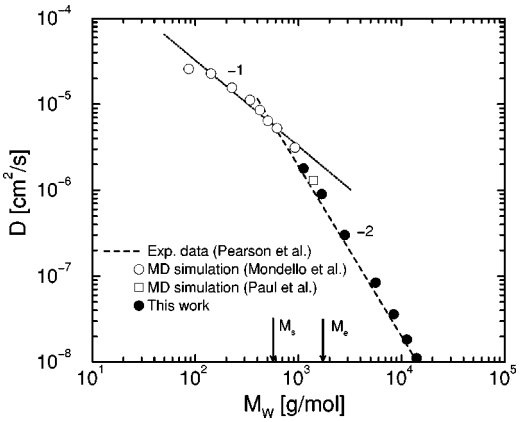

FIG. 14. Diffusion coefficient D vs molecular weight M_w for polyethylene from different simulation studies (open symbols) and experiment (long dashed line) compared to the present simulation results (closed circles). All simulations were carried out at constant density. The crossover between two scaling regimes is indicated by the arrow labeled with M_s.

$$\tau_0^{\mathrm{CG}} = \tau_{N-1}^{\mathrm{eff}} = \left[4 W_{N-1}^{\mathrm{eff}} \sin^2\left(\frac{(N-1)\pi}{2N} \right) \right]^{-1} \approx [4 W_{N-1}^{\mathrm{eff}}]^{-1}, \tag{16}$$

where we have added the superscript CG to indicate that it depends on the level of coarse-graining. The approximation in Eq. (16) is valid in case N is large compared to unity. From Fig. 8(a) we estimate $W_{N-1}^{\mathrm{eff}} \approx 2.8\ \mathrm{ns}^{-1}$, which yields $\tau_0^{\mathrm{CG}} \approx 0.09$ ns. This is in good agreement with the transition from t^1 to $t^{1/2}$, as observed in Fig. 13.

The observed minimal slope of 0.4 is not as low as the reptation prediction of 0.25. There are two reasons, which are both related to averaging. First, in going from the atomistic to the blob level we average over some of the atomic movement. Since the mean square displacement of a blob is always less than the mean square displacement of a more detailed particle, but relatively larger differences occur at shorter times, the scaling laws of the blobs are less pronounced than one would expect for more detailed particles.[5] Secondly, we have averaged over all the blobs. It is well known that, because of contour length fluctuations, the entanglement constraints are more easily released at the chain ends than at the inner section of a chain. This was shown in simulations of the FENE polymer model by Kremer and Grest.[11] The pure reptation result will only hold for very long chains where the influence of the chain ends is relatively unimportant. Recently, Pütz *et al.* performed simulations of up to 10 000 beads per chain, in which case a minimal slope of 0.26 was observed with great clarity.[12] Our chain lengths are clearly not yet in this long chain limit.

More evidence for the existence of the slowing down length N_s can be found in the molecular weight dependence of the self-diffusion coefficient D. In Fig. 14 results by several authors, who performed simulations of *n*-alkanes and polyethylenes, are combined. The open circles are constant density ($\rho = 0.766$ g/cm^3) simulation results of C_6 to C_{66} alkanes at $T = 448$ K by Mondello *et al.*[2] The open square is a constant density ($\rho = 0.777$ g/cm^3) simulation result of C_{100} by Paul *et al.*[1] The latter has been corrected from $T = 509$ to 450 K, in the same way as described in Ref. 1 by using the result for the temperature dependence of the friction as obtained from an analysis of a C_{90} system by Pearson *et al.*, $\xi \sim \exp[1326/(T-149)]$.[28] The closed circles are results from this work, the calculation of which will be explained further on. The diffusion coefficient scales approximately like M_w^{-2} for the larger molecular weights. The low molecular weight data of Mondello *et al.* is more or less consistent with M_w^{-1}. We expect that the agreement with the Rouse model prediction is only fortituous in this regime where chain end effects dominate, as was shown by Harmandaris *et al.*[4] Nevertheless, the crossing over between these two regimes occurs at a molecular weight which is found to correspond well to the slowing down length, $M_s = N_s M \approx 560$ g/mol. Notice that all calculations were performed at approximately the same density, therefore ruling out the possibility that the increase in the effective friction is a density effect.

Pearson *et al.* have measured D in alkane and polyethylene melts at $T = 450$ K.[28] They found that the entire range from $M_w = 600$ to 120 000 follow a power law,

$$D^{\mathrm{exp}} = 1.65/M_w^{1.98} \quad (\mathrm{cm}^2/\mathrm{s}). \tag{17}$$

This fit is also plotted in Fig. 14 (dashed line). It is important to note that the experimental density is not constant, but increasing with molecular weight. However, the experimental density levels off to a value of 0.766 g/cm^3 relatively fast; from $M_w = 600$ onward the increase is $<5\%$.[28] We can therefore rule out density effects to explain the scaling in this experimental range, and the results can directly be compared with constant density simulations. It is clear from Fig. 14 that the simulation results agree well with Eq. (17). Below $M_w = 600$ there *is* a large increase in the experimental density, making the effective friction subject to density effects. This explains why the experimental scaling in this regime does not agree with constant density simulation results, such as those of Mondello *et al.*[2]

Pearson *et al.* corrected for the increase in friction factor in order to effectively keep the same distance from the glass transition temperature. He then observed a transition in the

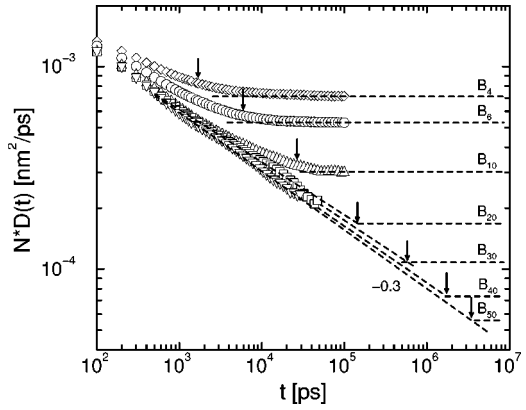

FIG. 15. Center-of-mass mean square displacement, scaled such as to represent a time-dependent diffusion coefficient $D(t)$, Eq. (19). The dashed lines show the extrapolations to the disentanglement times τ_d (arrows). The symbols are the same as in Fig. 9.

scaling of D at a molecular weight which was more in agreement with the entanglement weight M_e from rheological measurements.[28] In this work, however, we put ourselves to the viewpoint that the remaining increase of friction at constant density is a physical effect (we will not try to analyze whether it is a free volume effect or otherwise) that must be reproduced by any realistic simulation model. Indeed, the experimental data is reproduced, and we do not see a transition at M_e. In most other constant density simulation work the transition in D is wrongfully interpreted as the entanglement molecular weight, which may explain some of the discrepancies that arise when comparing with rheology. We will return to this in the discussion.

Now we will explain how the diffusion coefficients were calculated. To this end we will define the mean square displacement of the center-of-mass $\mathbf{R}^{\mathrm{cm}}$ of a chain;

$$g_{\mathrm{cm}}(t)=\langle[\mathbf{R}^{\mathrm{cm}}(t)-\mathbf{R}^{\mathrm{cm}}(0)]^2\rangle. \tag{18}$$

According to the Rouse model, $g_{\mathrm{cm}}(t)=6Dt$ for all times and $D\sim N^{-1}$. A real chain however will be severely hindered by the interactions with surrounding chains, leading to subdiffusive behavior. According to the reptation model, $g_{\mathrm{cm}}(t)\sim t$ up to the entanglement time τ_e, followed by $g_{\mathrm{cm}}(t)\sim t^{1/2}$ up to τ_r $(=\tau_R)$. Subsequently the chain diffuses along the quasi-one dimensional Gaussian tube contour which results in three dimensional diffusive motion of its center of mass with $D\sim N^{-2}$. We generalize the diffusion coefficient to a time-dependent diffusion coefficient, according to

$$D(t)=g_{\mathrm{cm}}(t)/6t, \tag{19}$$

with limiting value $D=\lim_{t\to\infty}D(t)$. The deviation from the Rouse model becomes most distinct if we plot $ND(t)$ against correlation time. This is shown in Fig. 15. If the Rouse model were valid, all data would be constant and fall on top of each other. This is clearly not the case; subdiffusive behavior is observed, and it apparently sets in even before τ_s, which was also observed in the work of Kremer.[11] The early subdiffusive behavior occurs for all chain lengths, including chains which are shorter than the entanglement length. This can be explained as a ''correlation hole'' effect in the polymer mode-coupling (PMC) theory of Schweizer.[29] In this theory an explicit nonlinear coupling of the collective fluid density fluctuations with the segmental density field of a probe (Rouse) polymer is introduced. The combined effect of chain connectivity and the correlation hole (induced by excluded volume interactions of the probe chain with the polymer matrix) cause the effective *inter*molecular interactions to be very long ranged, on the order of the radius of gyration of the polymer chain. This leads to a slow center of mass frictional memory decay and to subdiffusive behavior of $g_{\mathrm{cm}}(t)$. In fact, PMC theory predicts anomalously slow short time diffusion without *a priori* introducing the phenomenological tube concept. For relatively short times and chain lengths PMC theory explains the observed subdiffusive behavior well. For very long chains $g_{\mathrm{cm}}(t)\sim t^{9/16}$ is predicted, close to the reptation result. It will therefore be very difficult to discriminate between these theories by analyzing mean square displacement data.

In Fig. 15, the minimal slope of $g_{\mathrm{cm}}(t)$ is observed to decrease with increasing chain length. However, even for our largest chain lengths the $t^{1/2}$ regime of the reptation model is not strictly followed (nor the $t^{9/16}$ regime of PMC theory). For the chain lengths studied here the picture of a chain diffusing freely along a Gaussian primitive path is too strict and only some broad crossover to diffusion with an averaged slope (0.7 for B_{50}) remains. As said before, only the chain lengths $N<20$ actually reached the diffusive regime. It is clearly seen that for these chain lengths the transitions from subdiffusive to diffusive behavior (horizontal lines in Fig. 15) occur at the calculated times τ_r (arrows in Fig. 15), where the Rouse modes crossover from nonexponential to exponential relaxation behavior. For the other chain lengths $(20\leqslant N\leqslant 50)$, we have assumed that the crossover occurs at τ_r, which we have put equal to the estimated τ_d values. This is how we obtained the diffusion coefficients D, which by the nature of the approximation may be slightly underestimated.

E. Entanglement time from shear relaxation

We will now turn our attention to the rheologic properties of polymer melts. Much theoretical and simulation effort has been spent to predict or reproduce the zero shear relaxation modulus $G(t)$, which measures the relaxation of stress after applying a small step shear strain. Experimentally, its Fourier transform is measured by applying small oscillatory shear, yielding the storage and loss moduli, $G'(\omega)$ and $G''(\omega)$. A prominent feature of viscoelastic liquids is the plateau that appears in $G(t)$, signifying the elastic part of the relaxation behavior that sets in after a liquidlike initial relaxation. The initial relaxation is generally believed to more or less follow the Rouse model,[27]

$$G(t)=\frac{ckT}{N}\sum_{k=1}^{N-1}\exp(-2t/\tau_k), \tag{20}$$

where c is the number concentration of blobs. The crossover time between the Rouse and the plateau regime is identified as the entanglement time τ_e. In the reptation picture, the

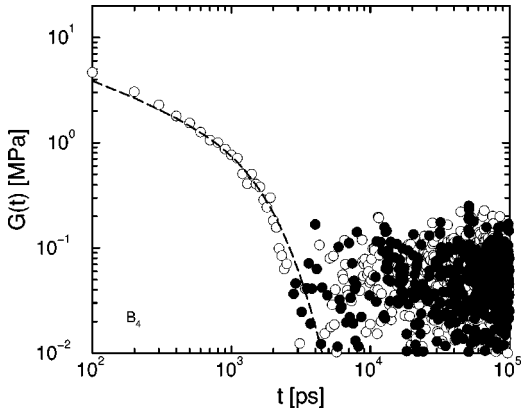

FIG. 16. Shear relaxation modulus of the B_4 system. Absolute values of negative data are represented by filled circles. The long dashed line is the Rouse model prediction, Eq. (20).

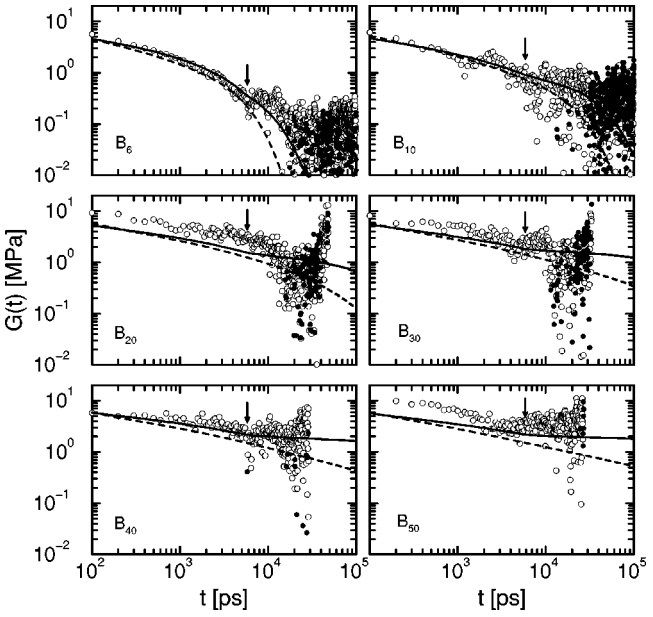

FIG. 17. Shear relaxation modulus of the systems with $6 \leqslant N \leqslant 50$, represented in the same way as Fig. 16. Arrows indicate the estimated entanglement time τ_e. The solid lines are predictions from a mixed Rouse and reptation approach, Eq. (24).

beads of the chain hit the tube wall at this time. In most simulation work, however, it has proved to be difficult to directly observe a plateau in $G(t)$.

The shear relaxation modulus was determined by autocorrelating nondiagonal elements of the stress tensor, as explained in a previous article.[10] The result for the B_4 system is shown in Fig. 16. Because the measuring time was finite, scattering of the data occurs at the largest correlation times where the relaxation modulus is close to zero. To assess the proximity to zero of the scattered data on a logarithmic scale, the positive data is represented by open circles and the negative data by closed circles. Where the number of open and closed circles are exactly balanced, the shear relaxation modulus is expected to be zero. The reader should be aware, however, that the closed circles are plotted in front of the open circles, which is why the closed circles may *appear* to dominate the open circles. Note that no effect is seen at the previously found slowing down time, $\tau_s \approx 0.47$ ns. In fact no entanglement effect is seen at all, and the data can very well be described by the Rouse model result, Eq. (20) and the dashed line in Fig. 16. Here we replaced τ_k with the measured effective relaxation time τ_k^{eff}, Eq. (11). In Fig. 17 we present the results for the systems with chain lengths $6 \leqslant N \leqslant 50$, in the same way as Fig. 16 (except for the solid lines; these will be explained later). Notice that already for B_6 a hump emerges after $t \approx 6$ ns which splits off the Rouse prediction (dashed line). In a previous article, we attributed this to a very slow relaxation of the interchain stress,[10] i.e., the hump indicates that we are in the transition region from unentangled to entangled dynamics. If we look at the other results in Fig. 17, we can observe how the hump evolves with increasing chain length. Although the data for $N=20$ and 30 may not be regarded conclusive (some oscillations remain), a rubbery plateau is observed for the two longest chain lengths studied, with hardly any negative data remaining.

Because the onset of entanglement effects is found in the B_6 system, we estimate the entanglement length to be $N_e \approx 6$. Also, we assume that the entanglement time is around the time at which the hump emerges: $\tau_e \approx 6$ ns. This entanglement time seems to be reasonable for $N>6$ as well (arrows in Fig. 17). The estimates of entanglement time and length are internally consistent if τ_e is interpreted as the relaxation time of a chain of length N_e: $\tau_1^{\mathrm{eff}}(N_e) \approx 5.7$ ns from Fig. 8(a). It is also very important that they are consistent with experimental results. It is encouraging to see that an entanglement molecular weight $M_e = 2000$ is predicted from neutron spin echo experiments on polyethylene by Richter *et al.* and Schleger *et al.*,[22,30] corresponding to $N=7$ blobs. Also, they predict an entanglement time of $\tau_e \approx 5$ ns at the slightly higher temperature of 509 K, in very good agreement with our observations. Most estimates of N_e from rheology are based on the magnitude of the plateau modulus instead of the onset of entanglement effects in $G(t)$. In the next subsection we will determine the value of the plateau modulus and compare it with rheological experiments.

F. Entanglement length from plateau modulus and viscosity

Let us consider the shear relaxation modulus $G(t)$ again (Fig. 17). For short times, $t < \tau_e$, the chain does not feel the entanglement constraints and behaves like a three-dimensional Rouse chain. It is usually assumed that the chains are Gaussian on all scales, i.e., that Eq. (6) applies, and that the modes relax exponentially at all times, together leading to Eq. (20). Real chains, as we have seen, behave differently. The agreement may be improved by explicitly accounting for the measured mode amplitudes, relaxation times, and stretching parameters. After some straightforward calculations [see, e.g., Eq. (4.145) in the book of Doi and Edwards,[27] and leave the equilibrium mode amplitudes explicit] we find

$$G(t)=\frac{c}{N}E\sum_{k=1}^{N-1}\langle \mathbf{X}_k^2\rangle \sin^2\left(\frac{k\pi}{2N}\right)\times\exp\left[-2\left(\frac{t}{\tau_k^*}\right)^{\beta_k}\right]\quad (t<\tau_e), \tag{21}$$

where E is proportional to the (entropic) spring constant. The value of E is unknown, but we assume that the pure Rouse model result, Eq. (20), is valid for t approaching zero. This leads to

$$E=(N-1)kT\left[\sum_{k=1}^{N-1}\langle \mathbf{X}_k^2\rangle \sin^2\left(\frac{k\pi}{2N}\right)\right]^{-1}. \tag{22}$$

For times $t>\tau_e$ the entanglement constraints are felt. According to the pure reptation model, the stress at time t is proportional to the fraction $\psi(t)$ of the original tube that is still part of the tube at time t,

$$\psi(t)=\sum_{k=\text{odd}}\frac{8}{k^2\pi^2}\exp\left(-\frac{k^2t}{\tau_d}\right). \tag{23}$$

According to Eq. (23) a well-defined plateau will emerge in the shear relaxation modulus if the chains are long enough. The summation is done over all odd k modes, usually with no upper limit. However, we expect that in reality only the first $k_{\max}\approx \text{int}(N/N_e)$ modes will contribute to the reptational part of the stress relaxation. The remaining modes correspond to scales which are smaller than the entanglement length, and are therefore expected to contribute to the stress relaxation in a Rouse-type fashion. Combining Eqs. (21)–(23), explicitly accounting for the measured relaxation times and stretching parameters in the reptational part also, we obtain the following prediction for the stress relaxation:

$$G(t)=F\sum_{k=\text{odd}}^{k_{\max}}\frac{8}{k^2\pi^2}\exp\left[-\left(\frac{t}{\tau_k^*}\right)^{\beta_k}\right]+\frac{c}{N}E\sum_{k=k_{\max}+1}^{N-1}\langle \mathbf{X}_k^2\rangle \sin^2\left(\frac{k\pi}{2N}\right)\times\exp\left[-2\left(\frac{t}{\tau_k^*}\right)^{\beta_k}\right]\quad (t>\tau_e), \tag{24}$$

where β_k must be replaced with 1 and τ_k^* replaced with τ_k^l if $t>\tau_r$. The constant F is determined in the usual way, by equating $G(t)$ right before [Eqs. (21) and (22)] and after [Eq. (24)] τ_e. The predicted results are shown as solid lines in Fig. 17. Although the simulation data cannot rigourously proof the validity of Eq. (24), the agreement is found to be rather good. The simulation results of B_{20} and B_{50} are somewhat too high, but we expect that longer averaging would have yielded results which are closer to the predicted lines.

The plateau modulus G_N^0 can be estimated from the value of the shear relaxation modulus at the entanglement time, $G_N^0\approx G(t=\tau_e)$. The estimated plateau values are plotted against molecular weight in Fig. 18. Clearly, the crossover from unentangled to entangled dynamics is made within the range of chain lengths studied: after the entanglement molecular weight of $M_e\approx 1700$ the plateau modulus quickly rises until it levels off to a molecular weight independent value which is in good agreement with the experimental value of 2.4 MPa.[32] To our knowledge this is the first time that the experimental plateau modulus of a specific polymer species has been reproduced with such good agreement by means of molecular dynamics simulations.

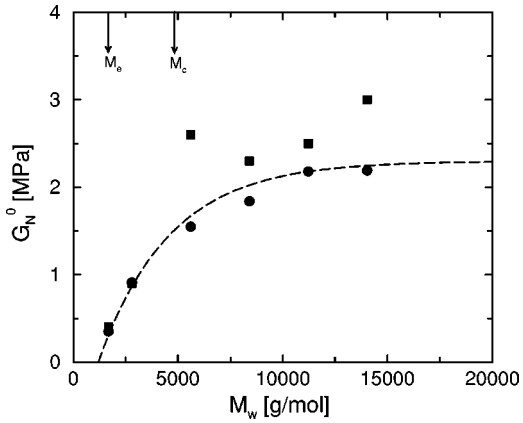

FIG. 18. Plateau modulus G_N^0, estimated from the simulation data (squares) and the mixed Rouse and reptation prediction, Eq. (24) (circles) vs molecular weight M_w. The dashed line is a guide to the eye.

In rheological practice, the entanglement molecular weight is calculated from the plateau modulus,[27]

$$M_{e,p}=\frac{4}{5}\frac{\rho RT}{G_N^0}, \tag{25}$$

in which R is the universal gas constant. We have added a subscript p to indicate that M_e is estimated from the plateau modulus. Using this, we find $M_{e,p}\approx 960$ ($N_{e,p}\approx 3.4$), which is between our previous estimate $M_e\approx 1700$ from the onset of entanglement effects in the shear relaxation modulus, and the slowing down molecular weight $M_s\approx 560$ from the Rouse mode and mean square displacement analysis. We will return to this in the Discussion.

The zero-shear viscosity can be calculated by integration of the shear relaxation modulus,[31]

$$\eta=\int_0^\infty G(t)dt. \tag{26}$$

Direct integration of the measured $G(t)$ data was possible for $N<20$. A comparison between the viscosities predicted by the Rouse approach, Eq. (20), and the mixed Rouse-reptation approach, Eq. (24), learns that the latter does a much better job in reproducing these values (see Table III). We will therefore rely on the mixed approach to predict the viscosities of the chain lengths $N\geqslant 20$. The results are shown in Fig. 19 (filled circles). Results by several other authors are given in Fig. 19 as well. The open circles are the constant density simulation results of C_6 to C_{66} alkanes by Mondello *et al.*[2] The open square is a constant density ($\rho=0.75$ g/cm^3) nonequilibrium dynamics simulation result of C_{100} by Moore *et al.*[3] Here we used their preliminary value of about 7.2 cP, obtained at the lowest shear rate of $\dot{\gamma}=1.5\cdot 10^8$ s^{-1}, which is expected to be in the Newtonian regime.

TABLE III. Tube diameter d^{NSE} from fits to the dynamic structure factor, plateau modulus G_N^0, viscosity η^{Rouse} based on the Rouse expression, Eq. (20), and viscosity η based on a mixed Rouse-reptation approach, Eq. (24) [viscosities determined by direct integration of $G(t)$ are between brackets], experimental viscosity η^{exp} (Ref. 28), diffusion coefficient D from the simulation, and experimental diffusion coefficient D^{expt} (Ref. 28). The last row gives experimental values for d^{NSE} for chain lengths B_{40} to B_{90} (Ref. 39), and the limiting plateau modulus for very long chains (Ref. 32).

N	d^{NSE} (nm)	G_N^0 (MPa)	η^{Rouse} (Pa s)	η	η^{expt}	$D(10^{-6}$ cm^2/s)	D^{expt}
4			0.004	0.005 (0.005)	0.006	1.8	1.5
6		0.35	0.008	0.011 (0.011)	0.013	0.90	0.68
10		0.91	0.019	0.033 (0.032)	0.034	0.30	0.25
20	6.9±0.9	1.55	0.056	0.20	0.17	0.084	0.063
30	5.3±0.4	1.84	0.14	0.88	0.73	0.036	0.028
40	5.2±0.5	2.18	0.30	2.95	2.09	0.018	0.016
50	5.8±0.5	2.19	0.51	5.98	4.68	0.011	0.010
Expt.	5.3±0.7	2.4					

Pearson *et al.*[28] found that at low molecular weight, $M_w < M_c \approx 5000$, the viscosity is well described by the power law,

$$\eta = 2.1 \cdot 10^{-5} M_w^{1.8} \quad (\mathrm{cP}), \tag{27}$$

while at high molecular weight, $M_w > M_c$, the M_w dependence is much stronger,

$$\eta = 3.76 \cdot 10^{-12} M_w^{3.64} \quad (\mathrm{cP}). \tag{28}$$

The crossover between the two regimes is determined by the critical molecular weight M_c, which, like the entanglement molecular weight M_e, is characteristic of the polymer species. We can understand the origin of M_c by noticing that at this molecular weight the plateau has almost fully developed, while at the same time τ_d has grown large enough for the reptation part to dominate the Rouse part of the integral of $G(t)$. However, the role of M_c may not be as fundamental as that of M_e: no characteristic time scale is connected with M_c and it is always equal to "a few times" M_e, enough for the entanglement effects to fully mature. For a more in-depth analysis of M_c the reader is referred to Ref. 32.

Pearson's fits, Eqs. (27) and (28), are plotted as dashed lines in Fig. 19. Notice the agreement between our simulation predictions and experiment. The results of Mondello *et al.*[2] show an initial regime where the viscosity scales with M_w, in agreement with pure Rouse model predictions. The crossing over to the $M_w^{1.8}$ regime occurs at the slowing down molecular weight M_s, i.e., at the same weight as where a crossing occurred in the scaling of the diffusion coefficient. Again, the results of Mondello *et al.* do not agree with those of Pearson *et al.* because they refer to different densities. Experimentally, there is a large increase in density in the region $M_w < M_s$, causing a faster than Rouse scaling of the viscosity. Trying to validate reptation theory, Pearson corrected the viscosity to the value it would have had if the friction factor had been constant (long chain limit). In that case the $M_w^{1.8}$ region disappeared and a new Rouse-type region was observed up to the critical molecular weight M_c. Given the agreement between our results and the experimental viscosities, and given the fact that above $M_w \approx 1000$ the density hardly changes, we can only conclude that Pearson's analysis must be on the wrong track.

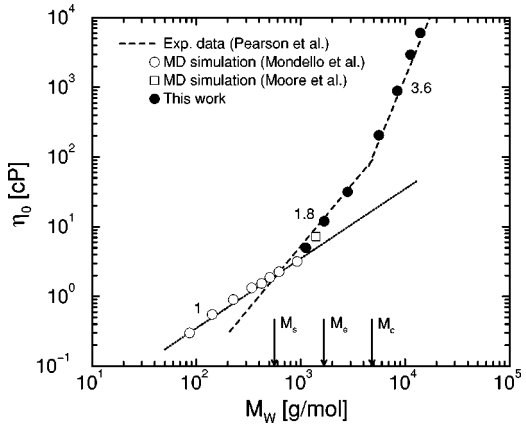

FIG. 19. The zero shear viscosity η_0 vs molecular weight M_w for polyethylene from different simulation studies (open symbols) and experiment (long dashed lines) compared to the present simulation results (closed circles). All simulations were carried out at constant density. The weights corresponding to different length scales are indicated by arrows.

G. Tube diameter from dynamic structure factor

The coherent dynamic structure factor can be measured by means of neutron spin echo spectroscopy. In the experiments conducted by Richter and co-workers, protonated chains were dissolved in a deuterated matrix.[22,30,33,34] Because the scattering lengths of protons and deuterons differ, they were able to extract the single chain coherent dynamic structure factor,

$$S(q,t) = \frac{1}{N_{\mathrm{sc}}} \sum_{i=1}^{N_{\mathrm{sc}}} \sum_{j=1}^{N_{\mathrm{sc}}} \langle \exp\{i\mathbf{q} \cdot [\mathbf{r}_i(t) - \mathbf{r}_j(0)]\} \rangle, \tag{29}$$

where $\mathbf{q}$ is the scattering wave vector and the double summation is over all N_{sc} scattering centers of one chain. Because our chains have been coarse-grained, detailed microscopic information about positions of the hydrogens is lost. However, it was shown in a previous article that, to a good approximation, the blob positions $\mathbf{R}_i$ can still be used in Eq. (29) to calculate the microscopic dynamic structure factor, provided the wavelength of the scattering wave vector is large compared to the bond length of bonded blobs.[10] As the maximum bond length is of the order of 2 nm, q will have to be small compared to 3 nm^{-1}. The results for five different

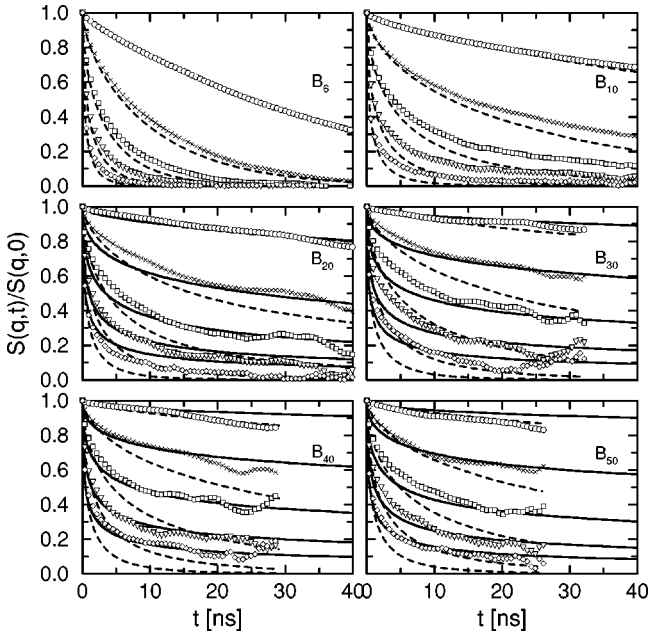

FIG. 20. Single chain coherent dynamic structure factors of the simulated chains. The q values shown are 0.55 nm^{-1} (circles), 1.0 nm^{-1} (crosses), 1.4 nm^{-1} (squares), 1.8 nm^{-1} (triangles), and 2.2 nm^{-1} (diamonds). Dashed lines are Rouse model predictions, Eq. (30), solid lines are fits to the reptation model, Eq. (31).

scattering vectors, $0.55 \leqslant q \leqslant 2.2$ nm^{-1}, are shown in Fig. 20 (symbols) for all chain lengths $N \geqslant 6$. We will now investigate to what extent this data is compatible with the Rouse and reptation models.

It was shown before that the simulation results of the B_6 system do not agree with the pure Rouse model predictions.[10] However, one might expect that the agreement improves if the mean square displacement of the center-of-mass and the mode amplitudes, relaxation times, and stretching parameters are taken explicitly into account, as we have done in the previous subsection. Inverting Eq. (4) and inserting in Eq. (29) yields

$$S(q,t)=\frac{1}{N}\exp\left\{-\frac{q^2}{6}\langle[\mathbf{R}^{\mathrm{cm}}(t)-\mathbf{R}^{\mathrm{cm}}(0)]^2\rangle\right\}\times\left\{\sum_{i=1}^{N}\sum_{j=1}^{N}\exp\left[-\frac{2q^2}{3}\sum_{k=1}^{N-1}\langle\mathbf{X}_k^2\rangle([A_{ki}-A_{kj}]^2+2A_{ki}A_{kj}[1-C_k(t)])\right]\right\}, \tag{30}$$

where it is assumed that the blob displacements are Gaussianly distributed and the Rouse modes remain orthogonal. A_{ki} and $C_k(t)$ are defined by Eqs. (5) and (13). The results from Eq. (30) are shown as dashed lines in Fig. 20. For all chain lengths, the fit for the smallest wave vector ($q=0.55$ nm^{-1}) is reasonably good. This wave vector is always small compared to $2\pi/R_g$, so only the overall center of mass motion is probed. Because this motion is explicitly introduced in Eq. (30), the good agreement comes as no surprise. The other wave vector results are in less good agreement. The modified Rouse prediction is observed to always underestimate the simulation results. This observation is in agreement with recent simulation and neutron spin echo work on unentangled 1,4-polybutadiene.[24] Smith *et al.* compared the dynamic structure factor results with a Rouse expression, modified in the same spirit as Eq. (30). They found that the failure of the Rouse model does not lie primarily in the predicted mode amplitudes or relaxation times, yet in the non-Gaussianity of segmental displacements. The non-Gaussianity is caused by chain-stiffness at the smallest scales and, more importantly, by intermolecular interactions at larger scales.

Above a certain chain length, the effects of intermolecular interactions become dominant in the form of entanglements. De Gennes[35] has formulated an expression for the single chain coherent dynamic structure factor, valid for times beyond τ_e and wave vectors much larger than the inverse end-to-end distance, i.e., $qR_e \gg 1$,

$$\frac{S(q,t)}{S(q,0)}=\{1-\exp[-(qd/6)^2]\}\exp(t/\tau_{\mathrm{loc}})\,\mathrm{erfc}(\sqrt{t/\tau_{\mathrm{loc}}})+\exp[-(qd/6)^2]\sum_{k=1}^{k_{\max}}\frac{A\sin^2(\alpha_k)}{\alpha_k^2(\mu^2+\alpha_k^2+\mu)}\times\exp\left(-\frac{4\alpha_k^2 t}{\pi^2\tau_d}\right), \tag{31}$$

where α_k are positive solutions of the transcedental equation,

$$\alpha_k\tan\alpha_k=\mu=\frac{q^2Nb^2}{12}, \tag{32}$$

and A is a normalization factor for the second term in Eq. (31). The first term describes the decay of correlations due to the smearing out of the (initially localized) chain throughout its tube. This is called local reptation. The associated q-dependent time scale τ_{loc} is given by

$$\tau_{\mathrm{loc}}=\frac{36}{Wb^4q^4}. \tag{33}$$

To calculate τ_{loc} is not trivial, because both the Rouse rate W and the effective statistical segment length b depend on the length scale. We can estimate these quantities by assuming that the length scale probed by a wave vector corresponds to the end-to-end distance of a subchain of some effective number (N_{eff}) of blobs, i.e., $N_{\mathrm{eff}}(q)b_{\mathrm{eff}}^2(q)\approx(2\pi/q)^2$. Using Fig. 3 we find that the effective number of blobs for the smaller scales are $N_{\mathrm{eff}}(2.2)\approx 3.6$ for $q=2.2$ nm^{-1}, $N_{\mathrm{eff}}(1.8)\approx 4.8$, and $N_{\mathrm{eff}}(1.4)\approx 7.0$, with effective statistical segment lengths $b_{\mathrm{eff}}=1.52$, 1.60, and 1.69 nm, respectively. From Fig. 8(a) the effective Rouse rates at these length scales are estimated as $W=0.43$, 0.32, and 0.25 ns^{-1}, respectively. This is very fortunate, for the product Wb^4 turns out to be almost constant: 2.27, 2.08, and 2.03 nm^4/ns, respectively. In our subsequent calculations we have used the average value of 2.1 nm^4/ns.

The second term in Eq. (31) describes the slow, global creep of the chain inside its tube, known as reptational diffusion. This process depends on the disentanglement time τ_d, which is known from the previous subsection. The summation is done over different reptational modes, and should

therefore stop at $k_{\max} \approx \mathrm{int}(N/N_e)$, while in the literature a value of either $N-1$ or ∞ is used. The difference, however, is small. It is important that the disentanglement times of long chains (say $N \geqslant 20$) are much larger than the entanglement time $\tau_e \approx 6$ ns. This causes a plateau to emerge at intermediate times $\tau_e < t < \tau_d$. It should be noted that in the original theory by De Gennes[35] the height of this plateau was determined by a prefactor $[1-(qd/6)^2]$, in which it was assumed that $qd \ll 1$. To allow for larger q values this prefactor is interpreted, in analogy with Schleger *et al.*,[30] as the first two terms in the Taylor series of $\exp[-(qd/6)^2]$.

The fits using Eq. (31) are shown as solid lines in Fig. 20. Since all other parameters were known from previous measurements, the tube diameter d served as the only fit parameter. For each chain length a joint fit for all q and $t > \tau_e$ was done. The dynamic structure factor results of the B_6 and B_{10} chains could not be described by Eq. (31) in any way. The results of the B_{20} system could be fitted reasonably well, except for the highest q value. The fit quality for the longer chains ($N > 20$) is good, particularly if we take into account that the chains are not extremely far in the entangled regime (only 5 to 8 times N_e). In a similar way, Pütz *et al.* have measured the dynamic structure factor of their FENE model chains.[12,36] They also found good agreement with reptation theory for chain lengths above 550, which is about 8 times N_e, if the proper[36] entanglement length is used (see the discussion, Sec. IV).

With this data, however, we are not able to distinguish between De Gennes' reptation model and other models which also predict a plateau, such as the rubberlike model of des Cloizeaux[37] or the model of Ronca.[38] Schleger *et al.* were able to show that experiment clearly favors the reptation model.[30] This was possible because they measured up to times as large as 175 ns. The correlation times of our simulations did not reach so far, but we have shown that the dynamic structure factor results are at least compatible with reptation. The tube diameters which follow from the fits are given in Table III. Notice that roughly the same tube diameter d is found for chain lengths $N = 30$, 40, and 50. Some scatter in the data of d occurs, but the average of $d \approx 5.4$ nm for the three largest chain lengths is in very good agreement with the results of Wischnewski *et al.* who found $d = 5.3 \pm 0.7$ nm for a similar molecular weight range, but at a slightly higher temperature.[39]

IV. DISCUSSION

In this work we have studied the time and length scales which determine the transition from unentangled to entangled dynamical behavior by means of coarse-grained molecular dynamics simulations. What have we learned from these simulations? First, we found clear evidence for stretched exponential relaxation of the Rouse modes. Our simulations show that the stretching parameter β_k depends on the length scale under consideration, but a constant value of 0.8 is observed for the first Rouse mode of each chain length between 6 and 50. If this value would remain the same for much longer chains, this would open up a way to roughly estimate the disentanglement times of long chains from relatively short simulations. As τ_r starts to deviate from τ_d, this estimate becomes increasingly worse. Moreover, there is, no guarantee that the value of 0.8 will persist indefinitely for longer chains. This must be investigated in future work.

It must be remarked that the nonexponential relaxation of the Rouse modes comes as no surprise. Stretching was already observed in our previous work on B_6,[10] but we did not pay attention to the fact that relaxation after τ_r is exponential, obtaining averaged estimates of the stretching parameters, which were somewhat closer to unity. Also, Richter *et al.*[22] suggested some years ago that the assumption of exponential decay for the Rouse modes may be too rough for higher molecular weight chains, which was confirmed by computer simulations.[1,23,24] However, the physical origin of the stretching is not entirely clear. Because stretching is observed at length scales below the entanglement length, a successful theory of polymer dynamics must not only include entanglement effects but possibly also other intermolecular correlations and chain stiffness effects. In this respect it is important to mention polymer mode-coupling theory[29] which predicts an intermediate time regime of non-exponential relaxation of the normal mode time correlation functions.

For the range of chain lengths studied here, we have made a rather detailed analysis of the scaling of the effective relaxation times with chain length N and mode number k. When plotted against N/k we find three universal regimes. In the first regime the effective relaxation times scale as predicted by the Rouse model, Eq. (8). The second regime is relatively small, but a distinct $(N/k)^4$ scaling can be observed around N_s. This k-dependence (k^{-4}) was predicted by Kavassalis and Noolandi in their Generalized Rouse Model (GRM), if we interpret their N_e as our N_s, but they find a different N-dependence (N^3).[40] Alternatively, the bending force model of Harnau *et al.*[41] could be used in an effort to explain the observed scaling as a stiffness effect. In our previous work on B_6,[10] we found that a stiffening of the chain caused both faster relaxation of the small scale modes and slower relaxation of the large scale modes. However, as was already pointed out by Richter *et al.*,[34] a stiffness correction alone is not enough. Using realistic values of the stiffness, the relaxation times decrease too slowly with increasing mode number. In our previous work we showed that the uncrossability of chains is an important factor in the internal relaxation of a polymer chain. It has a large influence on the relaxation times of all scales but the very smallest. From the deviation of the stretching parameters from unity, Fig. 7, we deduce that the kinetic constraints, caused by the uncrossability constraints, are most severe at length scales of the order of N_s. Although at this length scale we cannot yet speak of global entanglement effects (in the sense of confined dynamics inside a tube), there are strong local effects leading to a rapid increase of effective friction. The universality of the curves show that the magnitude of this effective friction depends on the absolute length scale and not on the chain length itself. This is also the case for the third regime, where the effective relaxation times scale like $(N/k)^3$. The third regime starts at about $1.5N_s$, i.e., C_{60}. While we can not rule out the possibility that the scaling of the second

regime only shows up in this particular coarse-grained model, the physical reality of the third scaling regime is supported by similar observations in other simulation models.[1,23,42] In all these simulations the density was kept constant. If the density is allowed to decrease with decreasing chain length, e.g., by simulating under normal pressure, the scaling of the relaxation times in each of these regimes is expected to be different. However, the characteristic length scales at which the transitions occur may still be observed. Indeed, Harmandaris *et al.*[4] performed atomistically detailed NVT simulations of polyethylene at $P=1$ atm, and found a clear increase of the friction coefficient between C_{40} and C_{60}. After the three universal regimes a final regime sets in where the effective relaxation times scale with $N^{3.5}$ and k^{-2}, in agreement with reptation theory if contour length fluctuations are included. Note that the smallest length scale where this final regime applies closes in on the largest available length scale ($=N$) with increasing chain length. They will merge at some very large chain length unless the observed scaling laws change beyond the range of chain lengths studied here.

If focus is laid on the terminal relaxation times, instead of effective relaxation times, the observed scaling is compatible with the reptation model for all length scales beyond N_e.

The effect of the increased friction around the length scale N_s shows up in the mean square displacement of blobs $g(t)$ as a transition from the initial Rouse-type $t^{1/2}$ behavior to a smaller power law exponent. In our case the exponent is about 0.4 for the B_{50} system, but lower values may be reached if longer chains are used and the average is taken over inner blobs to exclude the influence of the more mobile chain ends.[11,12] It is important to note that this transition occurs at an earlier time than the entanglement time. Likewise, the scaling of the diffusion coefficient with chain length (at constant density) displays a transition at N_s, not at N_e. If we study the mean square center of mass displacement $g_{\mathrm{cm}}(t)$, it becomes clear that the center of mass motion of a chain is strongly influenced by the uncrossability constraints. A subdiffusive regime is observed up to the time τ_r, which, because of the relatively short chain lengths studied here, almost coincides with the disentanglement time τ_d. To illustrate the consistency of putting τ_r equal to τ_d for the longer, but still not very long chain lengths, we have plotted in Fig. 21 the mean square displacement of the center-of-mass of a B_{40} chain and its extrapolation with slope 0.7. The extrapolation at $t=\tau_d$ exactly equals the mean square radius of gyration R_g^2, in agreement with the fact that the chain must have escaped its original tube at $t=\tau_d$. We note that in order for $g_{\mathrm{cm}}(\tau_d)=R_g^2$ to hold, the diffusion coefficient D must be proportional to R_g^2/τ_d, in which case a stronger than N^{-2} dependence is predicted. Indeed, a least squares fit to a power law of the data of $20\leqslant N\leqslant 50$ gives $D\sim N^{-2.2}$, which is in agreement with recent results giving $D\sim N^{-2.28\pm 0.05}$ for different polymer species.[43]

The advantage of coarse-graining bottom-up is that it allows for a direct comparison with atomistic simulations and experimental values, without any need of mapping to theoretical or phenomenological models. In our previous

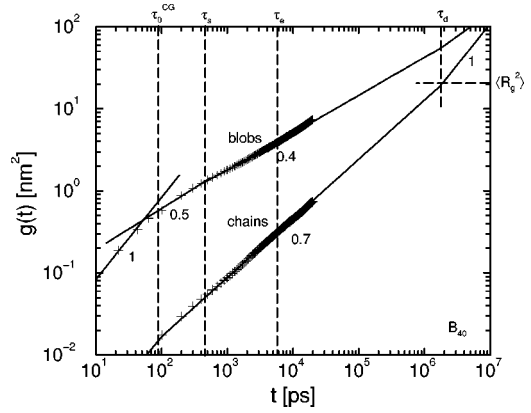

FIG. 21. Blob and center-of-mass mean square displacement data of the B_{40} system (plus). Extrapolation (solid lines) to $t=\tau_d$ yields a center-of-mass mean square displacement equal to $\langle R_g^2 \rangle$. Different time scales are indicated by dashed lines.

work we showed the good agreement between the coarse-grained and atomistic simulations[10] and in this work we showed the good agreement with experimental values. In Table IV the entanglement parameters found in this paper are summarized and compared with rheological and NSE data. The tube diameter for polyethylene as estimated from $S(q,t)$ ($d\approx 5.4$ nm) agrees well with experimental values for a similar molecular weight range. For very long chains, assuming that $d^2\approx N_e b^2$, we expect a tube diameter of $d^{\mathrm{NSE}}\approx\sqrt{6\cdot 3.3}=4.4$ nm, in agreement with (but slightly underestimating) the experimental value.[39] The plateau modulus yields an entanglement molecular weight which is about half of the estimate from $S(q,t)$, also in agreement with experimental observations. The reason why $M_{e,p}$ may differ from M_e was discussed by Tanaka *et al.*[44] They argued that $M_{e,p}$, defined by Eq. (25) is not a pure entanglement parameter, and may therefore not be the same as M_e, which is a parameter specifying the reptation/tube model.

Besides comparing with experimental work, we can also compare with other simulation work. The best studied simulation model of the last decade has been the FENE model of Kremer, Grest, and co-workers.[11–13] One of the remaining puzzles of this model is the discrepancy between the entanglement length N_e calculated from the mean square displacement and from the single chain coherent dynamic structure factor. Pütz *et al.* wonder why $S(q,t)$ should give different results from $g(t)$ since "they both are single chain quantities and measure the same motion." [12] However, the

TABLE IV. Entanglement parameters for PE from this simulation study ($T=450$ K) and experiment.

	Simulation	Experiment
τ_e (ns)	6	5[a]
M_e (g/mol)	1700	2000[a]
$M_{e,p}$ (g/mol)	960	920[b]
d^{NSE} (nm)	5.4	5.3[c]

[a]Estimate from NSE experiments at $T=509$ K (Ref. 30).
[b]From G_N^0, Eq. (25), including factor 4/5 at $T=443$ K (Ref. 32).
[c]For M_w 12000–25000; $d\approx 4.6$ nm for $M_w=36\,000$ (Ref. 39).

coherent dynamic structure factor measures the motion of a q-dependent number of chain segments surrounding the original position of a given segment. It is therefore sensitive to relative motions on a q dependent scale. On the other hand, the mean square displacement $g(t)$ measures the absolute motion of a single segment in space, and is therefore much more sensitive to local changes of the effective friction, resulting in a somewhat earlier slowing down. Thus, we suggest that the claimed entanglement length from $g(t)$ is actually the slowing down length N_s. (In this respect it is important to note that their simulations were also performed at constant density.) Pütz *et al.* deduced from the mean square displacement of (inner) segments an entanglement length (now slowing down length) of 35 segments for $N=700$ and 28 segments for $N=10\,000$.[12] The transition in the scaling of the diffusion coefficient with chain length also occurs around $N=35$ (see their Fig. 8 in Ref. 11). Fitting the single chain coherent dynamic structure factor $S(q,t)$ of the reptation model to their simulation data they find $d^{\mathrm{NSE}}=12.9\sigma$ for $N=700$ and $d^{\mathrm{NSE}}=9.6\sigma$ for both $N=2000$ and $N=10\,000$. The $S(q,t)$ data of $N=10\,000$ was found indistinguishable from that of $N=2000$,[36] from which may be concluded that finite chain length effects have no discernable effects beyond $N=2000$.[45] Again assuming that $d^2\approx N_e b^2$, this yields an entanglement length of $N_e^{\mathrm{NSE}}\approx(9.6/1.28)^2=56$ for very long chains. These estimates yield a ratio N_s/N_e^{NSE} of about 0.5 to 0.6, in rough agreement with the value of 0.33 expected for our simulation model in the case of very long chains. A second characteristic ratio to compare both models is $N_{e,p}/N_e^{\mathrm{NSE}}$. Pütz *et al.* estimated G_N^0 from the normal stress decay in a step strain elongation.[12] The outcome depended somewhat on the applied stress–strain formula, but an average yielded $N_{e,p}=72$ (65–83). Thus the ratio $N_{e,p}/N_e^{\mathrm{NSE}}$ was found to be approximately 1.3, while our result is about 0.6. This should be compared to the experimental result of about 0.5 which can be calculated from the values in Table IV. It is encouraging to find that our model predicts a proportionality between these length scales which agrees with experiment.

We end this section with a remark concerning computation times. Large computational overhead is introduced by the rather complicated uncrossability constraint. Still, there is a clear speed-up compared with atomistally detailed simulations as is exemplified by the fact that we are able to reach larger correlation times with equal computational effort. The FENE model mentioned above, using conventional schemes, also reaches such large speed-ups, or even larger ones.[11,12] We think, however, that our model, since it is built on an undulging atomistic model, encompasses time and length scales in a much more realistic way than the FENE model in which several monomers are mapped into an unrealistically hard bead. In the limit of very long chains this objection will become less important, while at the same time the FENE calculations will most probably be much faster than the TWENTANGLEMENT calculations.

V. SUMMARY

The general picture that emerges from this work is that the dynamics of medium long chain lengths (C_{400}–C_{1000}) is in approximate agreement with reptation theory, with fluctuating contour length corrections when necessary, but that the approximation of a primitive path moving with great freedom in a tube is too strict. The chains are interacting with their neighbors on every length scale, down to the slowing down length N_s, leading to non-exponential relaxation for as long as it takes a chain to escape its original environment. Only after time τ_r, equal to τ_d in the case of our moderately long chains, and for mode numbers smaller than $k_{\max}=\mathrm{int}(N/N_e)$, exponential relaxation occurs. This can effectively be accounted for by explicitly introducing into the reptation model results the measured relaxation behavior of the reptating modes. The same must be done with those modes whose length scales are smaller than the entanglement length, and which must be treated like Rouse modes. Proper care also has to be taken of the fact that the chains are not Gaussian, caused by stiffness and other sources of nonharmonicity. These effects can in some cases be handled by using measured mode amplitudes instead of pure Rouse amplitudes.

We want to stress that in our approach we started from the bottom, i.e., all coarse-grained parameters were determined "*ab initio*" from short atomistic molecular dynamics runs of polyethylene. The choice of the number of monomers in one blob, $\lambda=20$, was arbitrary within certain bounds, as explained in Sec. II. Other values, such as $\lambda=10$ or $\lambda=30$ could have been used, leading to different blob interactions, but they should lead to the same dynamic behavior. We find very good agreement with experimental data on polyethylene, which we think is to a large extent due to the way we have introduced the entanglements in our model. In contrast, if the uncrossability of chains is realized by combining relatively hard spheres into flexible chains, the proportionalities between different length scales may not be the same as those that occur in real polymer systems. Chemically realistic polymers are flexible only at large length scales when the beads will be almost empty and consequently very soft. These objections will become less important if one is interested only in very long time scales in very long polymer chains, in which case other, more conventional, coarse-grained simulations may become preferable.

We hope that the present work will aid in the understanding of the dynamics and rheology of polymer melts. It will certainly be interesting to extend this simulation model to even longer chains, possibly of different polymer species, and to investigate the nonlinear properties under shear.

ACKNOWLEDGMENT

This work is part of the research programme of the Stichting voor Fundamenteel Onderzoek der Materie (FOM), which is financially supported by the Nederlandse Organisatie voor Wetenschappelijk Onderzoek (NWO).

APPENDIX: DETERMINATION OF THE FRICTION FACTOR

In the coarse-grained approach the fast fluctuating interactions between the microscopic constituents are represented

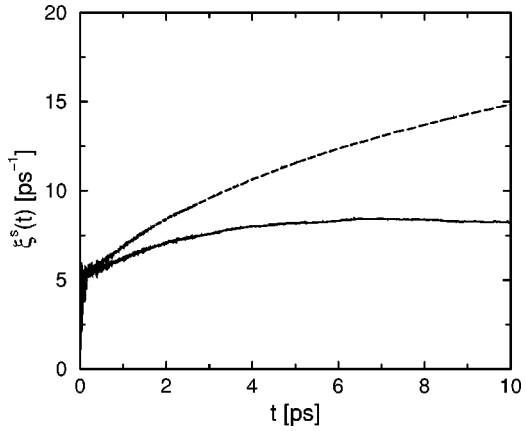

FIG. 22. Scalar friction from integration of the autocorrelation of the constraint force (dashed line) and autocorrelation of the random force (solid line), Eq. (A1). A value of $8\,\mathrm{ps}^{-1}$ was used in the coarse-grained simulations.

by random forces and frictions. Assuming that the friction on each blob is isotropic and independent of the positions of the other blobs, it can be calculated from

$$\xi(t)=\frac{\beta}{M}\int_0^t d\tau\langle F_\alpha^R(\tau)F_\alpha^R(0)\rangle, \tag{A1}$$

where $\beta=1/kT$ and F_α^R is the x, y, or z-component of the random force on a blob. The friction can be calculated from a microscopic molecular dynamics run.[46] To this end, a constraint force is added to fix the position of one blob relative to the center-of-mass of the box. Part of this force at each instant balances the mean force due to interactions with other blobs, while the remaining part balances the fluctuating random force due to the bath variables. The issue now is to isolate the latter part. Simply subtracting the long time average from the constraint force will not give the correct random force, because on the longer time scales the mean force also fluctuates, albeit at a much lower frequency. A way to estimate the maximum frequency with which the mean force oscillates is to search for the maximum curvature within one kT from the free energy minimum,

$$M\omega_{\max}^2\simeq(\nabla^2\chi)_{\max}. \tag{A2}$$

Applying this to the interaction model for our coarse-grained polyethylene blobs, we found $\omega_{\max}\simeq 0.06$ rad/ps. The constraint force was measured for five nanoseconds in a simulation of $C_{120}H_{242}$. The constraint force data was Fourier transformed and frequencies $\omega<\omega_{\max}$ were removed. The autocorrelation, Eq. (A1), was determined by squaring and Fourier transforming back to the time domain. Different blobs were fixed in different runs, to account for varying friction factors at different positions along the chain. However, it was found that these friction factors do not differ much for C_{120}. The averaged result is given in Fig. 22 (solid line). Notice that the friction levels off to a value of about $8\,\mathrm{ps}^{-1}$ after about 5 ps of correlation time, which was the value used in all our coarse-grained simulations. The 5 ps correlation time is sufficiently small compared to the smallest mean force oscillation period (about 100 ps), so the assumption that the blobs are slow compared to the bath variables (Markov approximation) seems to be justified. Figure 22 also shows the integrated autocorrelation of the constraint force itself (dashed line). In this case the friction factor becomes much larger, consistent with the fact that now also the interactions between the blobs, especially between blobs on different chains, are included in the friction. This leads to the well-known Einstein result for the diffusion coefficient,

$$D=\frac{kT}{NM\xi}, \tag{A3}$$

where N is the number of blobs in a chain. In Ref. 5 it was found that the friction frequency corresponding to the measured diffusion coefficient of a C_{120} chain must be $19.0\,\mathrm{ps}^{-1}$, which is consistent with our present results.

[1] W. Paul, D. Y. Yoon, and G. D. Smith, J. Chem. Phys. **103**, 1702 (1995); W. Paul, G. D. Smith, and D. Y. Yoon, Macromolecules **30**, 7772 (1997); W. Paul, G. D. Smith, D. Y. Yoon, B. Farago, S. Rathgeber, A. Zirkel, L. Willner, and D. Richter, Phys. Rev. Lett. **80**, 2346 (1998).
[2] M. Mondello and G. S. Grest, J. Chem. Phys. **106**, 9327 (1997); M. Mondello, G. S. Grest, E. B. Webb III, and P. Peczak, *ibid.* **109**, 798 (1998).
[3] J. D. Moore, S. T. Cui, H. D. Cochran, and P. T. Cummings, J. Non-Newtonian Fluid Mech. **93**, 83 (2000).
[4] V. Harmandaris, V. G. Mavrantzas, and D. N. Theodorou, Macromolecules **31**, 7934 (1998); **33**, 8062 (2000).
[5] J. T. Padding and W. J. Briels, J. Chem. Phys. **114**, 8685 (2001).
[6] P. E. Rouse, J. Chem. Phys. **21**, 1273 (1953).
[7] M. Fixman, J. Chem. Phys. **95**, 1410 (1991).
[8] J. Gao and J. H. Weiner, Macromolecules **25**, 1348 (1992).
[9] N. Fatkullin and R. Kimmich, JETP Lett. **69**, 762 (1999).
[10] J. T. Padding and W. J. Briels, J. Chem. Phys. **115**, 2846 (2001).
[11] K. Kremer and G. S. Grest, J. Chem. Phys. **92**, 5057 (1990).
[12] M. Pütz, K. Kremer, and G. S. Grest, Europhys. Lett. **49**, 735 (2000).
[13] M. Kröger and S. Hess, Phys. Rev. Lett. **85**, 1128 (2000).
[14] S. W. Smith, C. K. Hall, and B. D. Freeman, Phys. Rev. Lett. **75**, 1316 (1995); J. Chem. Phys. **104**, 5616 (1996).
[15] T. Kreer, J. Baschnagel, M. Müller, and K. Binder, Macromolecules **34**, 1105 (2001).
[16] J. Gao and J. H. Weiner, J. Chem. Phys. **103**, 1614 (1995).
[17] J. T. Padding and W. J. Briels, TWENTANGLEMENT User's manual (Twente University, 2000).
[18] J. D. McCoy and J. G. Curro, Macromolecules **31**, 9362 (1998).
[19] H. Fukunaga (personal communication).
[20] Y. Masubuchi, J.-I. Takimoto, K. Koyama, G. Ianniruberto, G. Marrucci, and F. Greco, J. Chem. Phys. **115**, 4387 (2001).
[21] W. J. Briels, *Theory of Polymer Dynamics*, Lecture Notes, Uppsala (1994). The full text can be downloaded from http://www.tn.utwente.nl/cdr/PolymeerDictaat/.
[22] D. Richter, L. Willner, A. Zirkel, B. Farago, L. J. Fetters, and J. S. Huang, Phys. Rev. Lett. **71**, 4158 (1993).
[23] J. S. Shaffer, J. Chem. Phys. **103**, 761 (1995).
[24] G. D. Smith, W. Paul, M. Monkenbusch, and D. Richter, J. Chem. Phys. **114**, 4285 (2001).
[25] K. L. Ngai, R. W. Rendell, A. K. Rajagopal, and S. Teitler, Ann. N.Y. Acad. Sci. **484**, 150 (1986); K. L. Ngai and J. Skolnick, Macromolecules **24**, 1561 (1991); K. L. Ngai, S. L. Peng, and J. Skolnick, *ibid.* **25**, 2184 (1992).
[26] W. Hess, Macromolecules **21**, 2620 (1988).
[27] M. Doi and S. F. Edwards, *The Theory of Polymer Dynamics* (Clarendon, Oxford, 1986).
[28] D. S. Pearson, G. Ver Strate, E. von Meerwall, and F. C. Schilling, Macromolecules **20**, 1133 (1987).
[29] K. S. Schweizer, J. Chem. Phys. **91**, 5802 (1989); **91**, 5822 (1989).
[30] P. Schleger, B. Farago, C. Lartigue, A. Kollmar, and D. Richter, Phys. Rev. Lett. **81**, 124 (1998).
[31] Analogous to Ref. 5 a small amount of 1.5 cP was added to account for the difference between the initial shear relaxation of atomistically detailed and coarse-grained systems.

[32] L. J. Fetters, D. J. Lohse, S. T. Milner, and W. W. Graessley, Macromolecules **32**, 6847 (1999).
[33] D. Richter, R. Butera, L. J. Fetters, J. S. Huang, B. Farago, and B. Ewen, Macromolecules **25**, 6156 (1992); D. Richter, B. Farago, R. Butera, L. J. Fetters, J. S. Huang, and B. Ewen, *ibid.* **26**, 795 (1993).
[34] D. Richter, M. Monkenbusch, J. Allgeier, A. Arbe, J. Colmenero, B. Farago, Y. Cheol Bae, and R. Faust, J. Chem. Phys. **111**, 6107 (1999).
[35] P. G. de Gennes, J. Phys. (France) **42**, 735 (1981).
[36] M. Pütz, K. Kremer, and G. S. Grest, Europhys. Lett. **52**, 721 (2000).
[37] J. des Cloizeaux, J. Phys. I **3**, 1523 (1993).
[38] G. Ronca, J. Chem. Phys. **79**, 1031 (1983).
[39] A. Wischnewski, D. Richter, M. Monkenbusch, L. Willner, B. Farago, G. Ehlers, and P. Schleger, Physica B **276–278**, 337 (2000).
[40] T. A. Kavassalis and J. Noolandi, Macromolecules **21**, 2869 (1988).
[41] L. Harnau, R. G. Winkler, and P. Reineker, Europhys. Lett. **45**, 488 (1999); Phys. Rev. Lett. **82**, 2408 (1999).
[42] K. Kremer, G. S. Grest, and I. Carmesin, Phys. Rev. Lett. **61**, 566 (1988).
[43] T. P. Lodge, Phys. Rev. Lett. **83**, 3218 (1999); H. Tao, T. P. Lodge, and E. D. von Meerwall, Macromolecules **33**, 1747 (2000).
[44] M. Tanaka, K. Iwata, and N. Kuzuu, Comput. Theor. Polym. Sci. **10**, 299 (2000).
[45] A. Wischnewski and D. Richter, Europhys. Lett. **52**, 719 (2000).
[46] R. L. C. Akkermans and W. J. Briels, J. Chem. Phys. **113**, 6409 (2000).